[American Journal of Science, Vol. 321, April, 2021, P. 393–423, DOI 10.2475/04.2021.01]

American Journal of Science

APRIL 2021

TERRESTRIAL BIOMARKER ISOTOPE RECORDS OF LATE QUATERNARY CLIMATE AND SOURCE-TO-SINK SEDIMENT TRANSPORT PROCESSES IN SOUTHWESTERN TAIWAN

QUEENIE CHANG*,†, MICHAEL HREN*, ANDREW T. LIN**, CLAY TABOR*, SHUN-WEN YU***, YVETTE ELEY§, and GREGORY HARRIS*

ABSTRACT. Fluvial sediments are important archives of paleoenvironments. However, variations in sediment production and transport processes greatly influence sediment geochemistry and resultant interpretations of ancient conditions. Tectonically-active tropical regions are particularly sensitive to climate feedbacks because these areas are often characterized by high precipitation rates, rapid erosion and short sediment residence times. We analyzed the hydrogen and carbon isotope composition of plant-derived *n*-alkanes ($\delta^2H_{n\text{-alkane}}$ and $\delta^{13}C_{n\text{-alkane}}$) in sediment cores along the Gaoping River-submarine canyon system in southwestern Taiwan to examine climatic and geomorphic controls on isotope geochemical signatures of fluvial sedimentary archives. These records span the last ~26 kyr and provide critical insight into the temporal and spatial variations in sedimentary biomarker isotopes within a source-to-sink system. Isotope data are coupled with new results from an iCESM 1.2 Earth System Model of precipitation isotopes during the last glacial-interglacial cycle. Biomarker isotope and modeling results support two important conclusions. First, biomarker isotope values change by ~10 to 15‰ in $\delta^2H_{n\text{-alkane}}$ and ~1 to 2‰ $\delta^{13}C_{n\text{-alkane}}$ in offshore SW Taiwan through the late Quaternary deglaciation. These shifts are consistent with iCESM predictions and other records from the South China Sea and are best explained by a shift in isotope hydrology due to regional warming and biologic responses to increased atmospheric pCO_2. Second, the $\delta^2H_{n\text{-alkane}}$ of biomarkers preserved in onshore sediments proximal to the mountain range is ~15 to 20‰ more negative than biomarkers deposited in offshore sites, and the temporal change in carbon isotopes exceeds that observed in the offshore deposits. The onshore core locality is proximal to the orogen and characterized by a mean elevation > 1 km compared to the offshore site, which has a mean catchment elevation of ~500 m. These data show that depositional setting and catchment hypsometry strongly bias the geochemical signature of sediments transported through the river system. The magnitude of isotopic variability generated by catchment geometry and sediment integration greatly exceeds the change associated with warming during deglaciation. This result suggests that catchment integration processes may play a similar or larger role in shaping fluvial geochemical records in tropical mountain systems than climatic factors.

Key words: Source-to-sink, n-alkane, surface processes, last deglaciation, hydrogen isotope, carbon isotope

* Department of Geosciences, University of Connecticut, Storrs, Connecticut USA
** Department of Earth Sciences, National Central University, Taiwan
*** Exploration and Development Research Institute, CPC Corporation, Taiwan
§ School of Geography, Earth and Environmental Sciences, University of Birmingham, United Kingdom
† Corresponding author: queenie.chang@uconn.edu

INTRODUCTION

Fluvial networks are a key component of orogenic systems that mediate the erosion and transport of sediments from source to sink (Milliman and Syvitski, 1992). River networks evolve in response to several factors, including uplift and erosion rate and the timing and amount of precipitation and runoff (Blum and Törnqvist, 2000). As a result, the dominant processes shaping river systems vary along the length of the river from source to sink. In the river headwaters, sediment production and erosion dominate whereas in the lower reaches, river systems can be characterized by deposition in the floodplain, delta, and offshore environments. These sediment deposition areas preserve geochemical records of environmental change and the tectonic forces operating within a catchment. However, different locations in the system have different erosion/accumulation features, sediment residence times, and catchment integration. These variables can bias geochemical records of catchment environments (Ponton and others, 2014; Romans and others, 2016). Thus, long-term geochemical records generated from sediment archives in different portions of a river system can show significantly different signals related to a combination of external climate/tectonic perturbations and their influence on catchment processes.

Recently, advances in the application of compound-specific stable isotopes have enabled the development of geochemical records of terrestrial paleoenvironment from both terrestrial and marine sediments (Galy and others, 2011; Sachse and others, 2012; Ponton and others, 2014; Zhuang and others, 2014; Diefendorf and Freimuth, 2017; Eley and Hren, 2018; Bliedtner and others, 2020). Plants and other terrestrial biota produce organic molecules distinctly associated with terrestrial sources (Eglinton and Hamilton, 1967). Specifically, *n*-alkanes with long, odd-number carbon chains (that is, n-C_{25} to n-C_{31}) are produced predominantly by terrigenous plants (Eglinton and Hamilton, 1967). These compounds are resistant to degradation and alteration during transport and burial and are abundantly preserved in sedimentary archives (Eglinton and Hamilton, 1967). Hydrogen isotopes of plant waxes reflect ambient water isotope composition during plant growth in addition to environmental factors such as plant-specific fractionation differences and responses to water stress (see for example, Sachse and others, 2012). Carbon isotopes of plant waxes generally reflect isotope fractionation during photosynthetic carbon fixation and factors that affect photosynthesis efficiency such as atmospheric CO_2 concentration and moisture availability (Körner and others, 1988; Schubert and Jahren, 2012; Diefendorf and Freimuth, 2017). In combination, these can provide a record of past climate and the integration of molecular components in a source to sink system. Numerous studies have utilized the hydrogen and carbon isotope composition of *n*-alkanes ($\delta^2H_{n\text{-alkane}}$ and $\delta^{13}C_{n\text{-alkane}}$) preserved within sediment archives to constrain changes in environments during major climate events (see for example, Liu and Huang, 2005; Tierney and others, 2008; Tierney and DeMenocal, 2013; Fornace and others, 2016; Loughney and others, 2020), mountain growth (for example, Polissar and others, 2009; Hren and others, 2010; Zhuang and others, 2014; Zhuang and others, 2015), and ecosystem turnover (for example, Eley and others, 2016; Liu and others, 2019). However, sediment production and transport processes can vary both spatially and temporally within an evolving river system. As a result, there remains uncertainty over how the organic molecular isotope signature of major environmental changes is reflected in different portions of a river system. This issue is particularly significant in tectonically-active tropical mountain systems characterized by rapid uplift, high rates of erosion, short sediment residence times, and rapid accumulation in depositional sites.

Taiwan is characterized by some of the highest surface uplift and erosion rates on the globe (Dadson and others, 2003; Fellin and others, 2017). Frequent floods and landslides induced by typhoons or earthquakes drive extreme sediment delivery

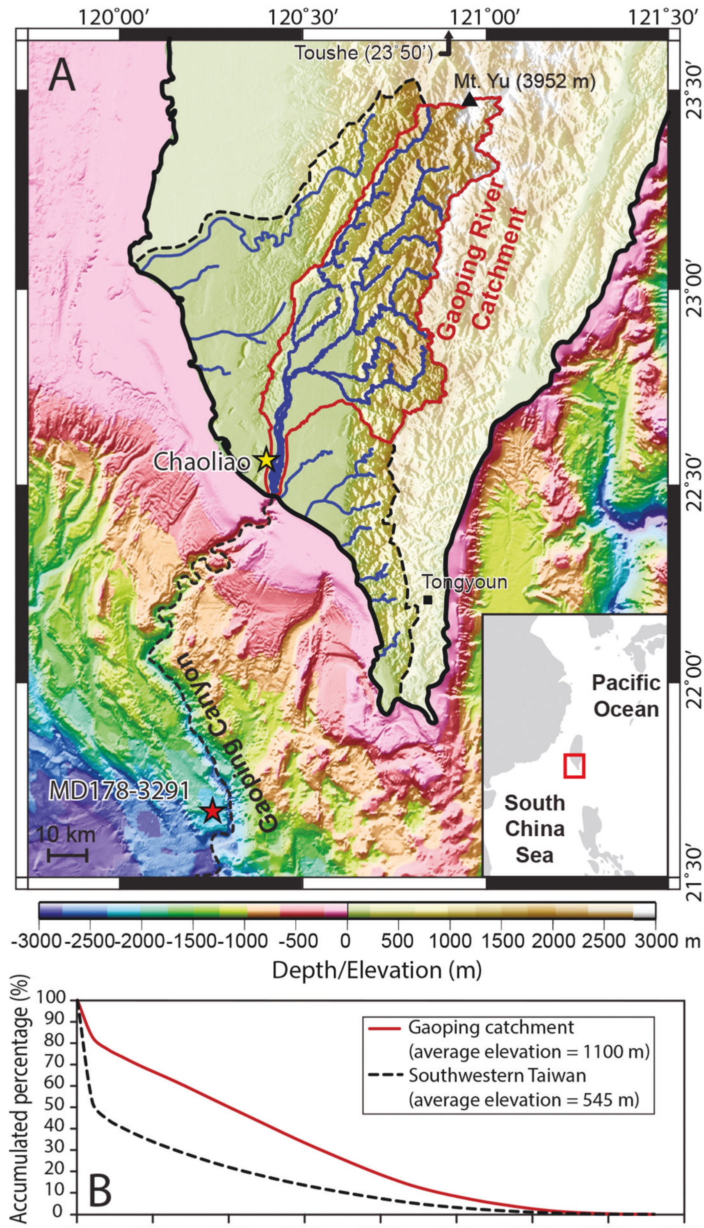

Fig. 1. (A) Topography and bathymetry map of the Gaoping River-submarine canyon system in southwestern Taiwan. The red star is the location of the offshore core (MD178-3291), and the yellow star is the location of the onshore core (Chaoliao). The red line outlines the catchment of the Gaoping River integrated by the onshore core, while the black dashed line delineates the catchments in southwestern Taiwan integrated by the offshore core. (B) The curves of the elevation distribution for the integrated catchment(s) of these two cores.

and export (Dadson and others, 2004; Hilton and others, 2008, 2011, 2012; R. Hsu and others, 2014; Yu and others, 2017; Zhang and others, 2018). As a result, Taiwan provides a natural laboratory to study the linkage and feedback among climate changes, sediment production and transport, erosion, and tectonic activities. Here we focus on the Gaoping River-submarine canyon system in southwestern Taiwan (fig. 1A), which is one of the most well-studied source-to-sink systems in Taiwan (Liu and others, 2002; Liu and Lin, 2004; Liu and others, 2010; Yu and others, 2017; Zhang and others, 2018). We sampled two sedimentary cores collected from onshore (Chaoliao) and offshore (MD178-3291) localities along the Gaoping River and Gaoping submarine canyon. These sediments record deposition and catchment processes since the last glacial period. We measured the hydrogen and carbon isotope compositions of fluvially-transported leaf-wax *n*-alkanes ($\delta^2H_{n\text{-alkane}}$ and $\delta^{13}C_{n\text{-alkane}}$). These data are paired with new and existing records of regional environmental change from the Last Glacial Maximum (LGM) to recent and a new water isotope-enabled version of the Community Earth System Model (iCESM 1.2). There are two goals of this work: (1) to examine how sedimentary organic molecular and stable isotopic records reflect the first-order environmental changes during the last deglaciation in Taiwan, and (2) to evaluate how geochemical records from different locations in the same catchment vary as a function of depositional setting and source-to-sink processes. Our data provide the first terrestrial isotope hydroclimate record of Taiwan from the LGM to recent and show that precipitation isotopes respond to warming of the regional climate since the LGM, rather than a simple change in precipitation amount. In addition, we show that onshore and offshore records of terrestrial LGM to recent environments vary as a function of sediment and organic molecular integration through the catchment.

GEOLOGICAL BACKGROUND

Gaoping River-Submarine Canyon System

The Gaoping River catchment is sourced from the highest mountain peak in Taiwan (Mt. Yu, 3952 m) and connects with the Gaoping Canyon, a well-developed submarine canyon with an extensive levee system and overbank deposits (Chiang and Yu, 2006, 2008; Yu and others, 2017) (fig. 1A). The Gaoping River delivers around 49 mega tons of sediments into the ocean every year (Dadson and others, 2003), making it the largest sediment source in southwestern Taiwan. Sediments are mainly delivered through landslides/debris flows triggered by extreme events such as earthquakes and typhoons (Dadson and others, 2004; Hilton and others, 2008, 2011, 2012; Zhang and others, 2018). The residence time of sediment within the river catchment is typically short due to the steep topography and high river discharge. The river discharge during typhoons in Taiwan can increase by two orders of magnitude (from <200 m^3/s to $>19{,}000$ m^3/s) and drop down to normal discharge within few days (Milliman and Kao, 2005; Kao and Milliman, 2008). As a result, sediments and organic material can be transported from terrestrial source to marine sink efficiently and with minimal time lag between erosion onshore and deposition offshore. Recent ^{14}C analysis of POC from the mouth of the Gaoping River shows that bulk organic carbon has an average age of ~2000 years, while *n*-alkanoic acids (fatty acids) from the same sediments yield an age of ~770 years (Eglington and others, 2021).

The Gaoping submarine canyon directly connects with the Gaoping River and the sediments within the submarine canyon are predominantly sourced from the Gaoping catchment. Modern *in situ* monitoring shows that terrestrial erosion within the Gaoping catchment during extreme events triggered by typhoons or earthquakes contributes over 70% of the total sediment delivered to the Gaoping submarine canyon as turbidity currents (Zhang and others, 2018). A smaller percentage of sediments deposited within the submarine canyon system may derive from materials remobilized by storm waves and sediment plumes from other nearby smaller river systems (Liu and others, 2002; Liu and Lin, 2004; Liu and others, 2009; F. Hsu and others, 2014). Therefore, while turbidity current-driven sedimentation is dominant in the Gaoping submarine canyon, offshore sediments associated with the submarine canyon are likely to represent a spatially-integrated record of sediment sourced from the SW Taiwan region.

Sedimentary Cores and Catchment Integration Differences

We analyzed fine-grained mud and silt deposits from two sediment cores in the Gaoping River-submarine canyon system: an offshore core (MD178-3291) located at the flank of the Gaoping submarine canyon and an onshore core (Chaoliao core) located on the modern floodplain at the river mouth of the Gaoping River (fig. 1A). Both cores span the past ~26 kyr, covering the period from LGM to the present.

The offshore core, MD178-3291, is a 33-m-long piston core spanning the last 26 ka, providing the longest and most complete sedimentary record in offshore southwestern Taiwan. This core was acquired in 2010, utilizing the R/V Marion Dufresne, and stored at 4 °C in Taipei Core Storage Center since collection. The age model for this core is established by nine planktonic foraminifera and plant fragment AMS ^{14}C (Yu and others, 2017) (fig. 2A). MD178-3291 is located at the western bank of the Gaoping submarine canyon, which is around 600 m higher than the canyon channel. This core is primarily composed of hemipelagic muds and laminated silt layers derived from overbanking turbidite flows that are less influenced by channel erosion and can provide continuous records (Yu and others, 2017). The sedimentary characteristics of this core are distinct below and above ~16 m. Below ~16 m, the sediments are primarily composed of mud with only a few turbidity currents layers, while above ~16 m, turbidites are thick and frequent. This sedimentology change reflects increased precipitation intensity and sediment supply due to deglaciation around 12 kyr (Yu and others, 2017).

The onshore Chaoliao core is a 220-m-long core located on the downstream floodplain of the Gaoping River, drilled by the Central Geological Survey of Taiwan in 1996. Age constraints for this core are reported by Chen (1998), including four plant fragments and organic-rich mud ^{14}C dates (5,070 ± 60 yr, 5,390 ± 50 yr, 6,530 ± 70 yr, and 15,360 ± 60 yr) and one thermoluminescence date (26 ± 4 kyr) (fig. 2B). The ^{14}C dating and calibration method reported in Chen (1998) is described in Chen and Liu (1996). The pollen records are reported by Liew (1998). A synthesis report (Shyu, ms, 1999) provides a description of sedimentology correlated with the pollen data. Below ~140 m, pollen data shows an ecosystem dominated by temperate forest species such as *Clobalanopsis, Alnus*, and *Gramineae*, indicating a climate characterized by lower temperature and mean precipitation than the present. Above ~140 m, pollen assemblages are dominated by tropical-subtropical forests and shrubs, such as *Euphorbia*, *Mallotus*, *Macaranga*, *Castanopsis*, and *Lysimachia*. This transition in vegetation types indicates a transition from the cold/dry glacial period to the warm/wet interglacial period (Liew, 1998). In addition, the lithology below ~140 m is comprised mainly of mud to silt of the floodplain to deltaic sands interlayered with mud/silt deposits. In comparison, above ~140 m, the sediment is dominated by gravels of the fluvial channel and alluvial fan deposits, reflecting an increase in sediment supply from the glacial to the interglacial period (Shyu, ms, 1999).

The sample locations of these two cores result in distinct differences in contributing sediment source area and hypsometry for the integrated upstream catchment. The onshore core, located at the river mouth of the Gaoping River and proximal to the orogen, integrates sediment and organic materials immediately from the Gaoping River. Here, upstream catchment mean elevation is 1100 m with over 50% of the catchment greater than 1000 m elevation (fig. 1B). In comparison, the offshore core is distal to the orogen and integrates significantly more low-elevation coastal plain area than the onshore cores site. The catchment mean elevation for the offshore

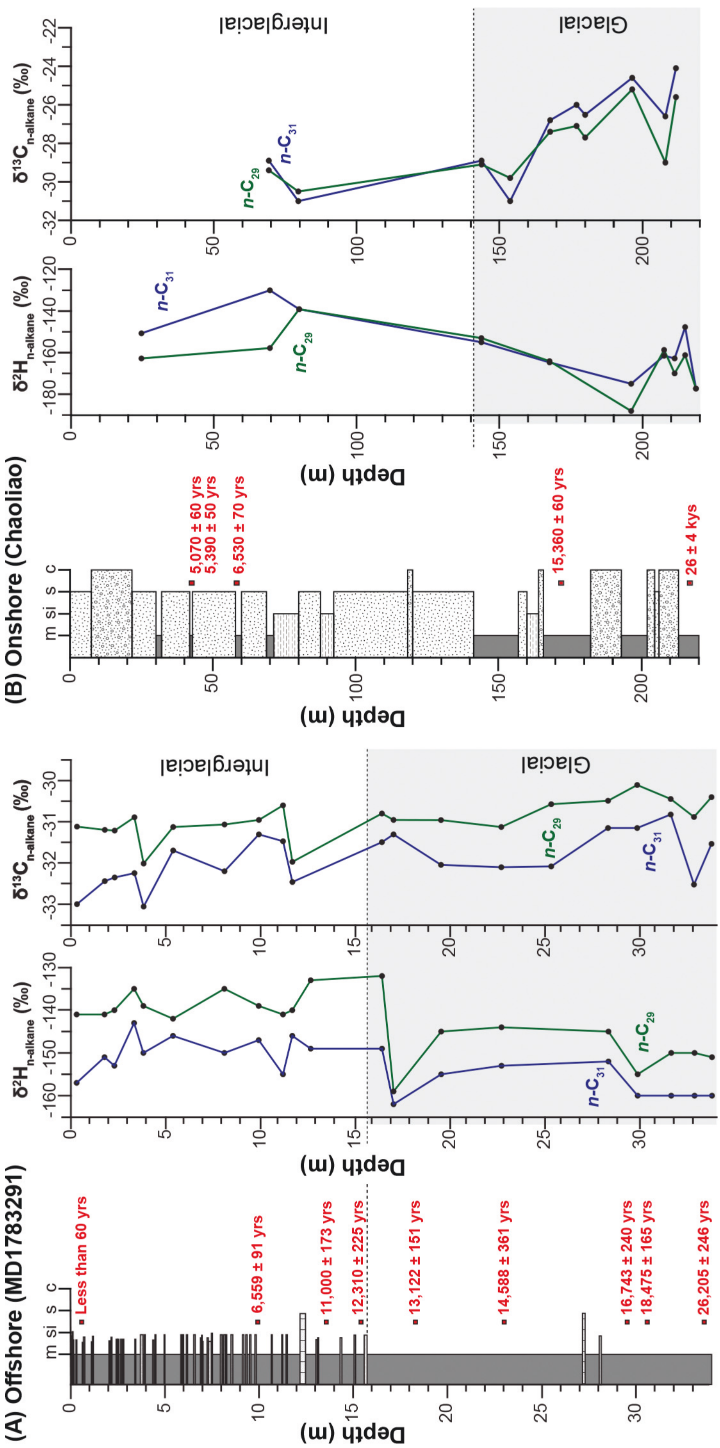

Fig. 2. Lithological description, age constrains, n-alkane stable isotope composition ($\delta^2H_{n\text{-alkane}}$ and $\delta^{13}C_{n\text{-alkane}}$) and distribution (CPI) of (A) offshore core (MD178-3291) (modified from Yu and others, 2017) and (B) offshore core (Chaoliao) (modified from Shyu, ms, 1999). The dashed line and gray shading separate the glacial and interglacial period deposits.

deposition site is ~500 m, with over 50% of the catchment lower than 100 m. The MD178-3291 offshore core is also located on the flank of the submarine canyon, so although the majority of sediments here are fed by the Gaoping River system (Liu and others, 2002; Yu and others, 2017; Zhang and others, 2018), this location may also receive fine-grained sediments discharged from nearby rivers and regionally dispersed through wave mixing on the inner shelf (Liu and others, 2002; Liu and Lin, 2004). As a result, sediments preserved in the offshore core site likely reflect a regionally-homogenized signal from across southwestern Taiwan.

METHODS

n-alkane Extraction and Separation

Samples were freeze-dried for 24 hours and powdered with mortar and pestle prior to Soxhlet extraction. Approximately 150 g of sediment was extracted for 48 hours using a 400 ml mixture of dichloromethane:methanol (2:1, v:v). The total lipid extracts (TLE) were saponified with 5 ml 1N KOH for 2 hours at 85 °C to detach the fatty acids from ester lipids. After saponification, the neutral lipid fraction (N1) was further separated through silica gel column chromatography. Columns were filled with around 1.5 ml activated silica gel and dried at 45 °C and rinsed with hexane thoroughly before loading the column with the N1 split. 2 ml hexane, 4 ml dichloromethane, and 4 ml methanol were added sequentially to elute the N1 to obtain the nonpolar, mid-polar, and polar fractions, respectively. After evaporative concentration, the nonpolar hexane fraction (S1) containing *n*-alkanes were further purified by urea adduction and silver nitrate ($AgNO_3$) chromatography to separate branched and cyclic alkanes. For the urea adduction, 200 µl urea-methanol solution, 200 µl pentane, and 200 µl acetone were added to the S1. The S1-containing fraction was frozen for at least 30 minutes to facilitate the crystallization of urea and compound adduction. The non-adducted fraction, which contains branched and cyclic alkanes, was removed with hexane, and the adducted fraction (A1), which contains *n*-alkanes, was then obtained by adding H_2O: methanol (1:1, v:v) to dissolve the urea crystal and extracted with hexane. For the silver nitrate chromatography, the A1 was applied using columns filled with around 1.5 ml $AgNO_3$ and eluted with 2 ml hexane.

n-alkane abundances were quantified on a Thermo Scientific Trace GC Ultra with a flame ionization detector (GC-FID), using a BP-5 column (30 m × 0.25 mm i. d., 0.25 µm film thickness) with helium as the carrier gas at a constant flow rate of 1.5 ml/min. Individual alkanes were identified by comparing their retention time to an internal laboratory standard mixture of *n*-C_7 to *n*-C_{40}. The peak areas of individual *n*-alkanes were used to calculate the carbon preference index (CPI) and average chain length (ACL) distributions using the following equations:

$$\mathrm{CPI} = \frac{1}{2}\left[\frac{(A_{C25} + A_{C27} + A_{C29} + A_{C31})}{(A_{C24} + A_{C26} + A_{C28} + A_{C30})} + \frac{(A_{C25} + A_{C27} + A_{C29} + A_{C31})}{(A_{C26} + A_{C28} + A_{C30} + A_{C32})}\right] \tag{1}$$

$$\mathrm{ACL} = \left[\frac{(A_{C25} \times 25 + A_{C27} \times 27 + A_{C29} \times 29 + A_{C31} \times 31 + A_{C33} \times 33)}{(A_{C25} + A_{C27} + A_{C29} + A_{C31} + A_{C33})}\right] \tag{2}$$

Compound Specific Stable Isotope Measurements

δ^2H and $\delta^{13}C$ values of *n*-C_{29} and *n*-C_{31} were determined using a GC-Isolink with a BP-5 column (30 m × 0.25 mm i.d., 0.25 µm film thickness), coupled to a Thermo Scientific MAT 253 isotope ratio mass spectrometer (IRMS). Compounds were separated on the GC with the temperature program set at 50 °C for 1 min, ramped to

180°C at 12°C/min, then ramped to 320°C at 5°C/min and held for 10 min. Isotopic compositions were standardized using a suite of *n*-alkanes from *n*-C_{16} to *n*-C_{30} in a standard mixture (Mix A6 from A. Schimmelmann). We determined internal and external precision by analyzing the standard for a range of sample sizes and repeat analyses of a single sample size. During the interval of measurement, the Mix A6 standard was analyzed every 4 to 5 samples to account for size and scale effects. Repeat analyses throughout the run and for a range of standard concentrations yield a precision of ~1 ‰ for $\delta^{13}C$ and < 5 ‰ for $\delta^{2}H$. All values are expressed in standard delta notation relative to VPDB and VSMOW.

Isotope-Enabled Climate Model

We utilize a water isotope-enabled version of the Community Earth System Model (iCESM 1.2) to simulate LGM and Pre-Industrial (PI) climate states to evaluate glacial to interglacial changes in isotope hydrology for comparison with biomarker isotope data. For this study, we configure iCESM1.2 with CAM5, CLM4, CICE4, and POP2 on 1.9x2.5° atmosphere and ~1° ocean grids. This configuration of CESM simulates PI and 20th century climate well (Hurrell and others, 2013). Further, the water isotope tracers of hydrogen and oxygen, which exchange through all interactive model components, compare favorably with observations (Nusbaumer and others, 2017; Wong and others, 2017). Several recent studies have employed iCESM for paleoclimate application (for example, Zhang and others, 2017; Zhu and others, 2017, Tabor and others, 2018).

Here, we produce two simulations: a PI control experiment and a LGM experiment. PI boundary conditions, including greenhouse gas (GHG) concentrations, land-sea mask, vegetation types, and orbit configuration, come from CESM defaults for 1850 CE. For the LGM, ice extent and topography come from the ICE-6G dataset (Peltier and others, 2015). Other LGM boundary conditions, such as GHG concentrations and orbital configuration, follow the PMIP3 protocol for 21 ka (Braconnot and others, 2012). To account for the large ice sheets, we increased ocean average $\delta^{18}O$ and $\delta^{2}H$ by 1‰ and 8‰, respectively (Duplessy and others, 2002). Both simulations were initialized from previously equilibrated experiments and run for an additional 550 years with water isotope tracers, allowing the atmosphere, land, and upper-ocean to reach near equilibrium. All initial ocean isotopic distributions come from the GISS interpolated ocean dataset (LeGrande and Schmidt, 2006). Analyses come from the final 48 years of simulation.

RESULTS

We measured the distribution of normal alkanes in both onshore and offshore cores to quantify average chain length and carbon preference indices. CPI values range from 0.9 to 2.5 and average chain lengths from 27 to 29.4 (fig. 2; table 1). The average CPI for the onshore core is around 1.9, while that of the offshore core is around 1.6. In general, low CPI values of *n*-alkanes could indicate a higher degree of microbial degradation or greater post-depositional thermal maturation (Eglinton and Hamilton, 1967; Vogts and others, 2009; Bush and McInerney, 2013; Brittingham and others, 2017; Wang and others, 2017). However, the observed CPI range of alkanes within the two sample cores is similar to the CPI value of modern soils in Taiwan (Hren and others, 2018). This may be a result of the high temperatures and rapid oxidation of soil organic matter in the tropical environment. Teunissen Van Manen and others (2020) show that soil CPI is directly correlated with mean annual temperature in tropical areas. For climates with a mean annual temperature > 22°C, observed soil CPI is generally less than 5, with numerous reports of values less than 2, similar to our sites. In the offshore core, there is no significant change in the observed CPI of *n*-

TABLE 1

Leaf-wax n-alkanes stable isotope composition and molecules distribution of the offshore core (MD178-3291) and onshore core (17TW-CL)

Sample	Core	Depth (m)	Age (ka)	n-alkanes δ^2H (‰)				n-alkanes $\delta^{13}C$ (‰)				CPI	ACL
				$\delta^2H_{n\text{-C29}}$	SD	$\delta^2H_{n\text{-C31}}$	SD	$\delta^{13}C_{n\text{-C29}}$	SD	$\delta^{13}C_{n\text{-C31}}$	SD		
MD178-3291-1	offshore	0.34	0.0	-141	1	-157	0	-31.1	0.0	-33.0	0.0	1.7	29.0
MD178-3291-2	offshore	1.81	0.9	-141	4	-151	2	-31.2	0.1	-32.4	0.1	1.7	28.2
MD178-3291-3	offshore	2.33	1.3	-140	7	-153	3	-31.2	0.1	-32.4	0.2	0.9	27.3
MD178-3291-4	offshore	3.37	2.0	-135	0	-143	3	-30.9	0.2	-32.2	0.1	1.0	27.0
MD178-3291-5	offshore	3.86	2.4	-139	13	-150	8	-32.0	0.1	-33.1	0.1	1.6	28.5
MD178-3291-6	offshore	5.42	3.4	-142	5	-146	4	-31.1	0.1	-31.7	0.1	1.1	26.5
MD178-3291-8	offshore	8.13	5.3	-135	2	-150	1	-31.1	0.0	-32.2	0.2	1.7	27.9
MD178-3291-9	offshore	9.94	6.6	-139	4	-147	9	-31.0	--	-31.3	--	1.4	26.9
MD178-3291-10	offshore	11.22	8.1	-141	8	-155	4	-30.6	0.1	-31.5	0.0	1.6	28.5
MD178-3291-12	offshore	11.71	9.4	-140	1	-146	3	-32.0	0.2	-32.5	0.2	1.6	28.3
MD178-3291-13	offshore	12.68	11.0	-133	1	-149	1	--	--	--	--	1.6	28.4
MD178-3291-14	offshore	16.44	12.6	-132	0	-149	1	-30.8	--	-31.5	--	1.6	28.4
MD178-3291-15	offshore	17.05	12.8	-159	2	-162	3	-31.0	--	-31.3	--	1.5	28.1
MD178-3291-16	offshore	19.56	13.5	-145	1	-155	5	-31.0	0.1	-32.0	0.2	1.7	28.9
MD178-3291-17	offshore	22.74	14.5	-144	6	-153	3	-31.1	0.1	-32.1	0.2	1.7	28.5
MD178-3291-18	offshore	25.38	15.4	--	--	--	--	-30.6	0.2	-32.1	0.2	1.8	29.1
MD178-3291-19	offshore	28.38	16.4	-145	2	-152	0	-30.5	0.0	-31.2	0.0	1.6	28.7
MD178-3291-20	offshore	29.92	17.4	-155	2	-160	4	-30.1	0.2	-31.2	0.0	1.7	28.0
MD178-3291-21	offshore	31.69	21.4	-150	2	-160	0	-30.4	0.2	-30.8	0.0	1.8	28.5
MD178-3291-22	offshore	32.92	24.5	-150	2	-160	4	-30.9	--	-32.5	--	1.8	28.1
MD178-3291-23	offshore	33.84	26.8	-151	0	-160	3	-30.4	--	-31.5	--	1.9	28.5
17TW-CL02	onshore	24.8	3.0	-163	10	-151	12	--	--	--	--	2.1	28.9
17TW-CL03	onshore	70.0	7.3	-158	--	-130	--	-29.4	0.1	-28.9	0.2	1.4	28.1
17TW-CL04	onshore	80.3	8.1	-139	4	-139	5	-30.5	0.4	-31.0	0.5	1.4	28.1
17TW-CL06	onshore	144.4	12.7	-153	3	-155	3	-29.1	0.2	-28.9	0.2	1.4	28.1
17TW-CL07	onshore	154.4	13.5	--	--	--	--	-29.8	1.0	-31.0	0.6	1.3	27.4
17TW-CL08	onshore	168.4	14.5	-164	6	-165	14	-27.4	0.7	-26.8	0.0	2.3	28.8
17TW-CL09	onshore	178.1	15.2	--	--	--	--	-27.1	1.4	-26.0	2.0	2.1	28.4
17TW-CL10	onshore	180.2	15.3	--	--	--	--	-27.8	2.0	-26.6	0.6	1.7	28.1
17TW-CL11	onshore	197.1	20.2	-188	7	-175	5	-25.2	1.0	-24.6	0.4	2.1	29.3
17TW-CL12	onshore	208.7	23.6	-159	3	-161	7	-29.0	--	-26.6	--	2.1	29.4
17TW-CL13	onshore	212.4	24.7	-170	2	-163	2	-25.6	1.2	-24.1	0.4	2.4	28.7
17TW-CL14	onshore	216.1	25.7	-161	--	-148	--	--	--	--	--	2.4	28.6
17TW-CL15	onshore	219.9	26.8	-177	7	-177	7	--	--	--	--	2.5	29.1

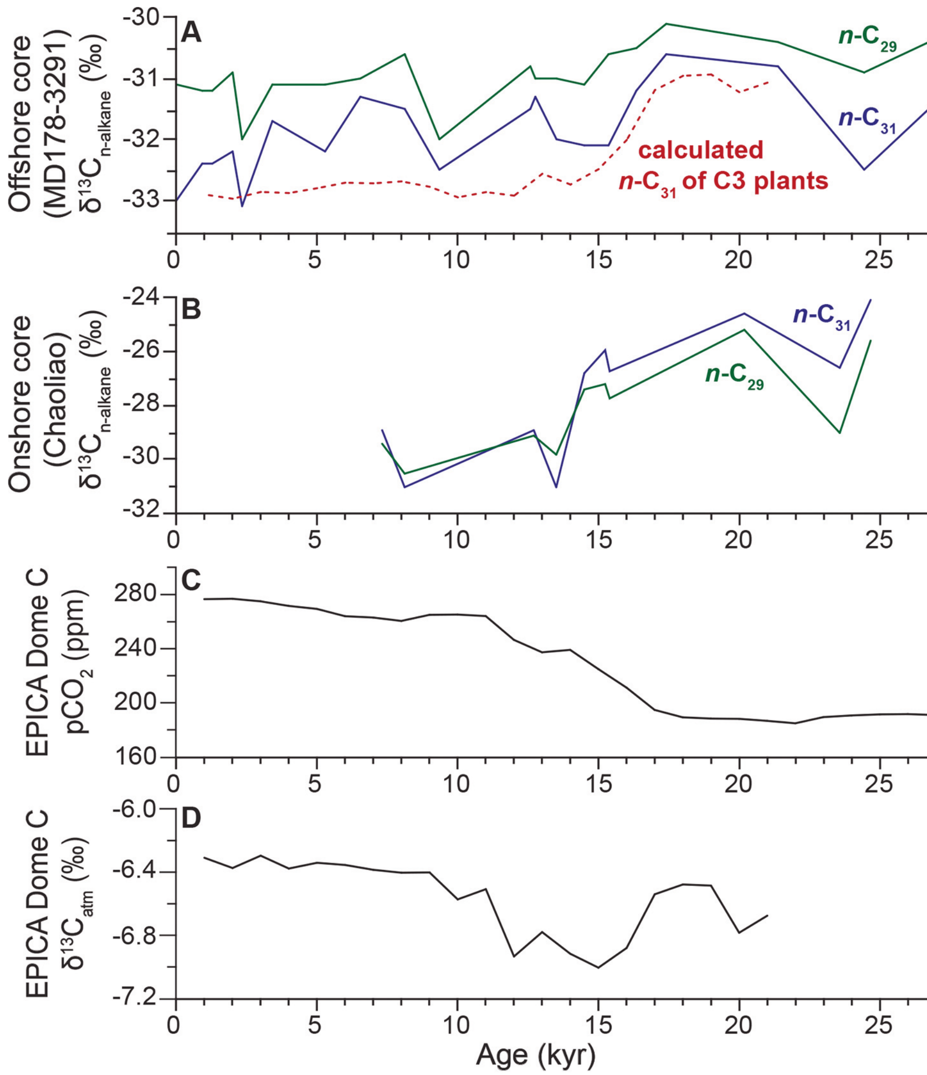

Fig. 3. (A) The $\delta^{13}C_{n\text{-alkane}}$ records of the offshore cores (MD178-3291) for both n-C_{29} and n-C_{31}. The red dash line represents the predicted $\delta^{13}C_{n\text{-}C31}$ variation through the last glacial-interglacial transition solely due to variation in atmospheric pCO_2 and $\delta^{13}C_{atm}$. Modeled value is based on the empirical equations (eq. 2 and eq. 3) proposed by Schubert and Jahren (2012); (B) The $\delta^{13}C_{n\text{-alkane}}$ records of the onshore cores (Chaoliao) for both n-C_{29} and n-C_{31}. (C) Global pCO_2 variation recorded in the ice core from EPICA Dome C, Antarctic (Elsig and others, 2009; Lourantou and others, 2010); (D) Global $\delta^{13}C_{atm}$ variation recorded in the ice core from EPICA Dome C, Antarctic (Lüthi and others, 2008).

alkanes from glacial to interglacial. In contrast, there is a shift from larger CPI values to smaller values from glacial to interglacial in the onshore record. There is a slight difference in CPI and ACL from onshore to offshore, with slightly smaller CPI and ACL values in the offshore core. However, the sediment cores for this study are all from terrestrial and shallow marine depths and there is no evidence for any thermal heating. As a result, there is no potential for differential diagenesis throughout the cores due to post-depositional heating. Any differences in CPI or ACL are presumed to result from source or climatic differences.

Compound Specific Stable Isotope Data

The carbon isotope composition of *n*-alkanes (*n*-C_{29} and *n*-C_{31}) for both the offshore core (MD178-3291) and onshore core (Chaoliao) are presented in figure 3 and table 1. The offshore core $\delta^{13}C_{n\text{-alkane}}$ shows an ~2‰ negative temporal shift from the glacial to the interglacial period for both *n*-C_{29} and *n*-C_{31}. $\delta^{13}C_{n\text{-C31}}$ is more negative than $\delta^{13}C_{n\text{-C29}}$ in general, with greater fluctuations (fig. 3A). The $\delta^{13}C_{n\text{-C29}}$ varies from between −31‰ to −30‰ during the glacial period and between −31‰ and −32‰ during the interglacial period. $\delta^{13}C_{n\text{-C31}}$ is mostly around −31‰ to -32‰ during the glacial period, and gradually decreases to −33‰ during the interglacial. In the onshore core, the magnitude of the carbon isotopic shift through the glacial-interglacial transition is larger than the offshore core (fig. 3B). An ~5‰ negative temporal shift is observed for both *n*-C_{29} and *n*-C_{31}. Unlike the offshore core, the $\delta^{13}C_{n\text{-C31}}$ in the onshore core is generally more positive than $\delta^{13}C_{n\text{-C29}}$. During the glacial period, the average $\delta^{13}C_{n\text{-C29}}$ is around −26‰ to −28‰, and the $\delta^{13}C_{n\text{-C31}}$ is around −25‰ to −27‰. During the interglacial period, the average $\delta^{13}C_{n\text{-C29}}$ is around −30‰ to −31‰, and the $\delta^{13}C_{n\text{-C31}}$ between −31‰ to −32‰. The $\delta^{13}C_{n\text{-alkane}}$ values of the onshore core are greater than the offshore core in general.

The hydrogen isotope composition of *n*-alkanes (*n*-C_{29} and *n*-C_{31}) in both the offshore (MD178-3291) and onshore core (Chaoliao) are presented in figure 4 and table 1. For the offshore core, the $\delta^{2}H_{n\text{-alkane}}$ for both *n*-C_{29} and *n*-C_{31} show an ~10‰ positive temporal shift from the glacial to the interglacial period (fig. 4A), while the $\delta^{2}H_{n\text{-C31}}$ is more negative than $\delta^{2}H_{n\text{-C29}}$. During the glacial period (prior to 17 ka), the $\delta^{2}H$ $_{n\text{-C29}}$ averages ~ −150‰ while during the interglacial period (after 12 ka), $\delta^{2}H_{n\text{-C29}}$ averages ~ −140‰. During the glacial-interglacial transition between 17 to 12 ka, a sharp negative shift in $\delta^{2}H$ is observed in both *n*-C_{29} and *n*-C_{31}. The timing of the negative isotope shift is consistent with a depositional age of around 12.9 ka using existing age models. Although this timing is coincident with the age of the Younger Dryas period, limited sampling in this interval and uncertainties in the precise timing of this event in the stratigraphic column make it difficult to precisely place this geochemical event in time.

The $\delta^{2}H_{n\text{-alkane}}$ values in onshore sediments are consistently more depleted than those preserved in an offshore depositional setting. In addition, the magnitude of the isotopic shift from glacial to interglacial is greater in onshore sediments than in offshore deposits (fig. 4B). $\delta^{2}H_{n\text{-C29}}$ values in the glacial period range from -160‰ to −180‰, and show an increase to −140‰ to −160‰ in the interglacial period. Mean $\delta^{2}H_{n\text{-C29}}$ values shift from ~−170‰ to around −155‰ from glacial to interglacial. Due to limitations of the age model of the Chaoliao core, the precise timing glacial-interglacial transition cannot be clearly tied to a specific, narrowed interval of the onshore core. However, both $\delta^{2}H_{n\text{-C29}}$ and $\delta^{2}H_{n\text{-C31}}$ record an increase in measured value up-section that is consistent with isotopic records from offshore.

Carbon Chain Length and Isotope Data

Onshore and offshore cores show a positive shift in $\delta^{2}H_{n\text{-alkane}}$ from the LGM to recent and a decrease in $\delta^{13}C_{n\text{-alkane}}$. However, in the offshore core, the $\delta^{2}H_{n\text{-C29}}$ is more positive than $\delta^{2}H_{n\text{-C31}}$, whereas in the onshore core the $\delta^{2}H_{n\text{-alkane}}$ and $\delta^{13}C_{n\text{-alkane}}$ are similar for both chain lengths. Typically, within the same plant group, *n*-alkanes with different numbers of carbon molecules show a similar isotopic response to climatic and environmental factors (Chikaraishi and Naraoka, 2003; Bi and others, 2005; Wang and others, 2013; Diefendorf and Freimuth, 2017). However, multiple studies demonstrate that plants of different vegetation groups produce a range of biomarkers with distinct molecular distributions. Furthermore, the $\delta^{2}H_{n\text{-alkane}}$ of C_3 trees and grasses are generally distinct, with grasses showing more negative $\delta^{2}H$ than trees

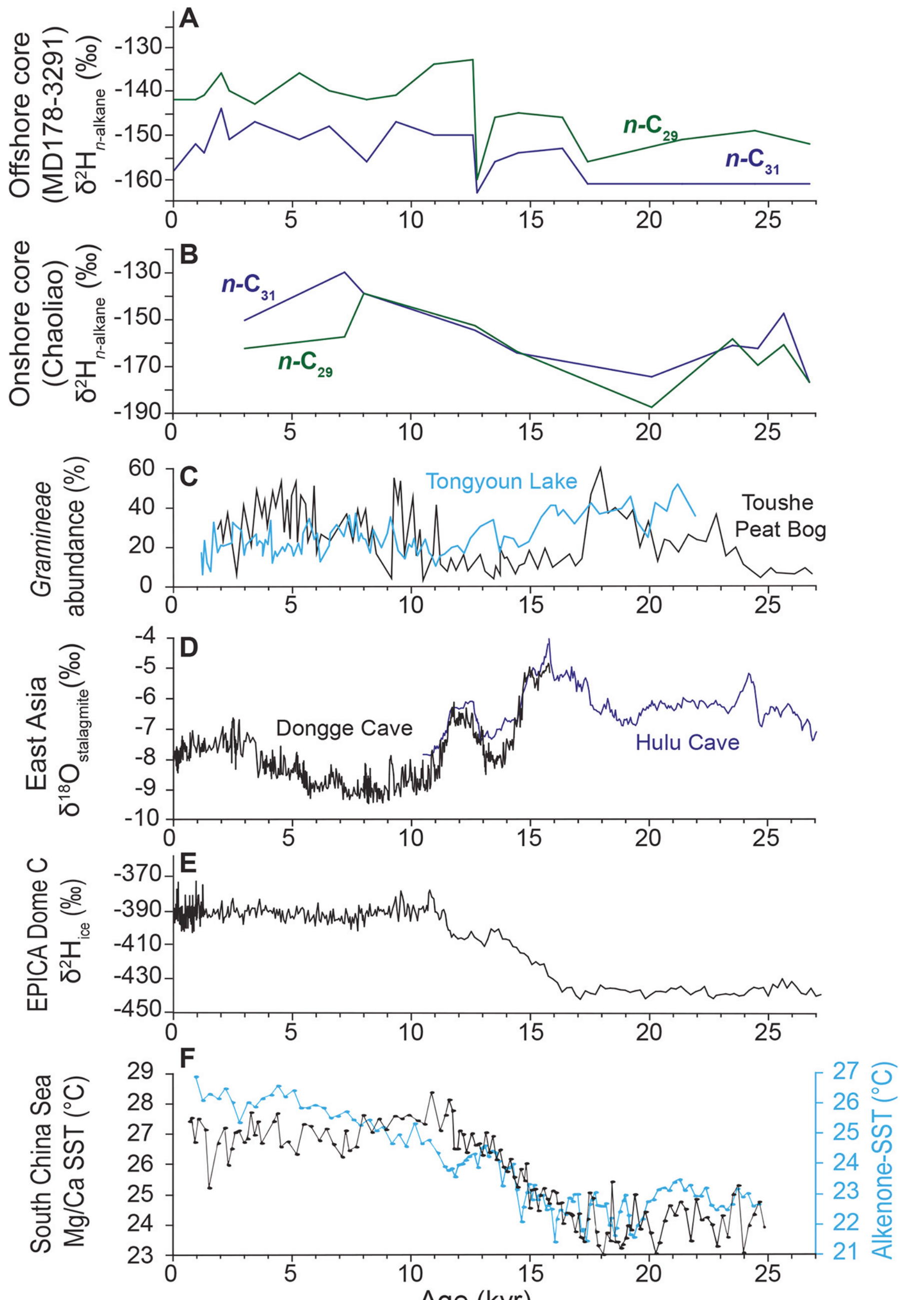

Fig. 4. (A) $\delta^2H_{n\text{-alkane}}$ records of the offshore cores (MD178-3291) for both n-C_{29} and n-C_{31}. (B) $\delta^2H_{n\text{-alkane}}$ records of the onshore cores (Chaoliao) for both n-C_{29} and n-C_{31}. (C) *Gramineae* pollen abundance in the Toushe Peat Bog core in central Taiwan (black; Liew and others, 2006) and Tongyoun Lake core (blue; Lee and Liew, 2010); (D) cave stalagmite $\delta^{18}O$ records from Dongge cave in southern China (black, Dykoski and others, 2005) and Hulu cave in central China (blue, Wang and others, 2001); (E) ice core δ^2H records from EPICA Dome C, Antarctic (Jouzel and others, 2007); (F) South China Sea Mg/Ca sea surface temperature (SST) records (Steinke and others, 2011) and Alkenone SST records (He and others, 2008).

(Sachse and others, 2012). Sachse and others (2012) compiled nearly 140 C_3 grass and tree samples and show a mean offset in $\delta^2H_{n\text{-alkane}}$ of ~35‰. Recent compilations of carbon isotopes of *n*-alkanes of C_3 trees and plants (Diefendorf and Freimuth, 2017), show considerable overlap between C_3 grass $\delta^{13}C_{n\text{-alkane}}$ values but an offset in mean $\delta^{13}C_{n\text{-alkane}}$ of only 1‰. Thus the hydrogen isotope composition of plant waxes from these two plant groups may show significant differences while carbon isotopes are similar.

In a source to sink system, *n*-alkanes preserved within fluvial sediments can have a mixture of vegetation sources. The contributions from different plant groups can change in response to climate or environmental factors or the variation in sediment provenance. For example, woody plants are shown to contribute proportionally more *n*-C_{27} and *n*-C_{29} than *n*-C_{31} or *n*-C_{33} compared to graminoids (grasses) which contribute proportionally more *n*-C_{31} and *n*-C_{33} alkanes (Vogts and others, 2009; Seki and others, 2010; Diefendorf and Freimuth, 2017). As a result, in regions with mixed forest and grass inputs, changes in the contributions from different vegetation types are likely to affect the $\delta^2H_{n\text{-alkane}}$ record of different carbon chain length molecules. Differences in the contributions from distinct vegetation types may be amplified by large-scale climatic changes or in sediment provenance within the catchment, especially for large catchments with a range of elevation.

Wang and others (2013) suggest that in an area with mixed grassland/forest vegetation, the δ^2H of longer chain *n*-alkanes such as *n*-C_{31} and *n*-C_{33} are sensitive to relative contributions of grasses. In contrast, since C_3-dicot forests may produce proportionally more *n*-C_{29} than longer carbon chain lengths, Wang and others (2013) suggest that δ^2H value of *n*-C_{29} are the most reliable record of paleo-precipitation δ^2H. Southwest Taiwan is characterized by a mixture of both grass and tree inputs and peat and lake cores from Central Taiwan show temporal changes in the abundance of graminoid pollen from the LGM to recent. We focus primarily on $\delta^2H_{n\text{-}C29}$ to evaluate the environmental influences on the *n*-alkanes isotope composition in southwestern Taiwan.

DISCUSSION

There are two important observations that result from new data presented here. The first is that $\delta^2H_{n\text{-alkane}}$ and $\delta^{13}C_{n\text{-alkane}}$ data from the offshore and onshore cores in the Gaoping River system show a temporal shift from LGM to the present. Thus, both onshore and offshore sediments record a geochemical change associated with a change in regional climate and/or catchment processes during the last deglaciation. The second is that onshore and offshore biomarker isotope records show differences in the baseline isotopic compositions of plant-derived biomarkers and the magnitude of isotopic change from the LGM to recent. The temporal shift in $\delta^2H_{n\text{-alkane}}$ and $\delta^{13}C_{n\text{-alkane}}$ reflects a change in environmental conditions and precipitation isotopes through the glacial-interglacial transition. In contrast, spatial differences in *n*-alkane isotope composition between the onshore and offshore cores most likely result from differences in catchment integration processes at depositional sites within the Gaoping River system.

Both onshore and offshore biomarker isotope records from the Gaoping River system record a decrease in $\delta^{13}C_{n\text{-alkane}}$ during the last deglaciation. The magnitude of this isotopic shift is significantly larger in fluvial sediments deposited near the orogen (onshore core), compared to sediments deposited in a marine, offshore component of the source-to-sink system. In addition, the onshore core is characterized by more positive $\delta^{13}C_{n\text{-alkane}}$ values than those preserved in the offshore setting. Hydrogen isotopes ($\delta^2H_{n\text{-alkane}}$) show a positive shift of 10 to 15‰ in both onshore and offshore sediments that occurs coincident with the transition from the LGM to

Holocene. However, the onshore biomarker $\delta^2H_{n\text{-alkane}}$ record is characterized by consistently more negative values than the offshore record. There are a number of processes that influence the hydrogen and carbon isotopic composition of plant-derived biomarkers. In some cases, factors that influence the carbon isotopic composition of plant biomarkers will also influence the hydrogen isotope composition. In other cases, these two geochemical signatures can change somewhat independently of one another. Here we discuss mechanisms for generating spatial and temporally-distinct isotopic signatures within the Gaoping River source-to-sink system for both carbon and hydrogen.

Leaf-Wax Carbon Isotopes

The carbon isotope composition of plants reflects fractionation between atmospheric CO_2 and leaf tissues during CO_2 diffusion into leaf stomata and during fixation within the leaf (O'Leary, 1981, 1988). The $\delta^{13}C$ value of plants can be affected by factors such as photosynthesis pathway (for example, Farquhar and Sharkey, 1982; Farquhar and others, 1989; Diefendorf and Freimuth, 2017), precipitation/water use efficiency (for example, Warren and others, 2001; Bowling and others, 2002; Diefendorf and others, 2010; Prentice and others, 2011; Eley and others, 2014; Eley and others, 2018), and atmospheric pCO_2 (for example, Farquhar and Sharkey, 1982; Beerling, 1996; Beerling and Royer, 2002; Schubert and Jahren, 2012, 2015). For carbon, the largest isotopic fractionation is due to the photosynthetic pathway (for example, C_3 versus C_4 or CAM photosynthesis pathways), followed by environmental factors that influence stomatal regulation. Sedimentary records of biomarker carbon isotopes can show variations that result from any combination of changes to these factors.

Atmospheric pCO_2 and $\delta^{13}C$ value.—The $\delta^{13}C_{atm}$ sets the starting isotopic composition for plant carbon (Tipple and others, 2010; Diefendorf and Freimuth, 2017) while the pCO_2 gradient between the atmosphere and the internal plant tissue influences stomatal regulation and the carbon fixation processes. In combination, these affect the magnitude of carbon isotope discrimination between atmospheric CO_2 and fixed carbon (for example, O'Leary, 1981, 1988; Farquhar and Sharkey, 1982; Farquhar and others, 1989; Ehleringer and Cerling, 1995; Beerling, 1996; Beerling and Royer, 2002; Schubert and Jahren, 2012, 2015). Schubert and Jahren (2012) proposed an empirical relationship between carbon fractionation ($\Delta\delta^{13}C$) and atmospheric pCO_2 for C_3 plants. For n-C_{31} alkanes, they show that the relationship between $\Delta\delta^{13}C_{n\text{-}C31}$ and pCO_2 can be described by the following equations:

$$\Delta\delta^{13}C_{n\text{-}C31} = \frac{34.3 \times 0.48(pCO_2 + 10)}{34.3 + 0.48(pCO_2 + 10)} \tag{3}$$

where

$$\Delta\delta^{13}C_{n\text{-}C31} = \left(\frac{\delta^{13}C_{atm} + 1000}{\delta^{13}C_{n\text{-}C31} + 1000} - 1\right) \times 10^3 \tag{4}$$

We use the reconstructed global carbon isotope composition of atmospheric $\delta^{13}C_{atm}$ of CO_2 (Elsig and others, 2009; Lourantou and others, 2010) and pCO_2 (Lüthi and others, 2008) from Antarctic EPICA Dome C ice core for the past 21 kyr to estimate the expected $\delta^{13}C_{n\text{-}C31}$ variation solely due to changes in atmospheric CO_2 concentration through time. Over the past 21 kyr, global atmospheric pCO_2 increased from ~180 ppm to ~280 ppm (fig. 3C), and $\delta^{13}C_{atm}$ from around −7.0‰ to −6.2‰ (fig. 3D). The calculated results (fig. 3A) show that $\delta^{13}C_{n\text{-}C31}$ of C_3 plants can be expected to vary from -31.0‰ to -33.0‰ over the past 21 kyr solely due to the increase in atmospheric pCO_2. This predicted ~2‰ negative temporal shift in $\delta^{13}C_{n\text{-}C31}$ during the glacial-interglacial transition is consistent with the variation observed in our $\delta^{13}C_{n\text{-}C31}$ records in the offshore core (fig. 3A). We suggest that the temporal shift in $\delta^{13}C_{n\text{-}C31}$ in the offshore core records in southwestern Taiwan primarily reflects the biologic response to changes of global $\delta^{13}C_{atm}$ and increasing pCO_2 from LGM to the present. In contrast, the temporal shift in onshore $\delta^{13}C_{n\text{-alkane}}$ from glacial to interglacial is larger than the expected change due solely to an increase of CO_2 from the LGM to recent. Furthermore, the $\delta^{13}C_{n\text{-alkane}}$ of the onshore core is generally more positive than the carbon isotope values observed in the offshore core. This requires mechanisms other than a change in pCO_2 or $\delta^{13}C_{atm}$ to explain the observed carbon isotope shift in the onshore record.

Vegetation change.—The single largest factor in shaping organic carbon isotopes in plants is the photosynthetic pathway. The $\delta^{13}C_{n\text{-alkane}}$ of modern C_4 plants generally range from −23‰ to −15 ‰ with a mean value of −20‰, while the $\delta^{13}C_{n\text{-alkane}}$ of modern C_3 plants generally range from −40‰ to −26‰ with an average value −35‰ (for example, Bi and others, 2005; Chikaraishi and Naraoka, 2007; Garcin and others, 2014; Diefendorf and Freimuth, 2017). Today, C_4 plants contribute ~ 30% of the total organic carbon to riverine sediments in southwestern Taiwan (Lin and others, 2020). However, sedimentary records suggest that there may have been significant changes in the proportion of C_3 and C_4 vegetation in Taiwan from the LGM to recent. For example, one bulk organic carbon isotope record from the Toushe peat core in central Taiwan shows a change from a $\delta^{13}C_{bulk}$ of −18‰ to −22‰ during the glacial period to around −26‰ to −28‰ during the interglacial period. This carbon isotope record was interpreted to show an increase in the relative abundance of C_3 plants from LGM to Holocene (Li and others, 2013). Similarly, data from core MD05-2905 in the south China sea show a decrease in $\delta^{13}C$ of ~4‰ from the LGM to recent, which was interpreted to reflect a shift in the proportion of regional C_4 input from ~60% to 40% of total alkane inputs (Zhou and others, 2012).

Our onshore *n*-alkane carbon isotope record is represented by relatively few points due to lithologic limitations but suggests up to a 5‰ negative shift in $\delta^{13}C_{n\text{-alkane}}$ from glacial to interglacial in contrast to a shift of only 1 to 2‰ in the offshore. Such a large change could be explained by a shift in the proportion of C_3 to C_4 plants contributing to the organic matter pool. Indeed, changes in vegetation cover may contribute to the magnitude of carbon isotope change observed in the Chaoliao core site. However, it is unlikely that the carbon isotope record simply reflects vegetation changes in the proportion of C_3/C_4 from LGM to recent. For example, to produce a ~5‰ shift in $\delta^{13}C_{n\text{-alkane}}$ would require up to ~40% C_4 plants in the contributing Gaoping River catchment. Distal marine core records (MD05-2905) have been interpreted to record changes of this magnitude in the abundance of C_4 plants in SE Asia. However, local Taiwan data does not indicate such a dramatic change from LGM to recent. Pollen records in Taiwan do not show a fundamental turnover in C_3/C_4 vegetation type throughout the last glacial-interglacial transition. In fact, records from central (Toushe peat bog) and southern (Tongyoun lake) Taiwan show a transition from temperate forest to the subtropical and tropical forest from the LGM to Holocene (Liew and others, 2006; Lee and Liew, 2010). These data suggest that even in the relatively arid glacial period, the tropical to the subtropical environment in Taiwan was wet enough to sustain a dominantly C_3 forest ecosystem. Thus a shift in the proportion of C_3/C_4 vegetation is unlikely to explain all of the observed temporal carbon isotope variability in the onshore record.

Precipitation.— Numerous datasets show that the carbon isotopic composition of leaves is correlated with mean annual precipitation (for example, Warren and others, 2001; Bowling and others, 2002; Diefendorf and others, 2010; Prentice and others, 2011). Increased mean annual precipitation generally produces smaller $\delta^{13}C_{n\text{-alkane}}$. This relationship may relate to differences in soil water content and moisture availability to vegetation, which ultimately influences stomatal regulation and carbon discrimination (Diefendorf and others, 2010; Diefendorf and Freimuth, 2017). Paleorainfall intensity indices inferred from the relative contribution of organic carbon and nitrogen in Tongyoun Lake in southern Taiwan show that rainfall intensity increased from the last glacial period to the present (Yang and others, 2011). This increase in precipitation during the last deglaciation could offer one potential explanation for the decrease in $\delta^{13}C_{n\text{-alkane}}$ values from LGM to the Holocene for both onshore and offshore sediments. However, the modern mean annual precipitation in Taiwan exceeds 2500 mm/yr and can be up to >3000 mm/yr in the mountain regions (for example, mean annual precipitation rate at Mt. Yu is 3600–4700 mm/yr). Pollen records show that LGM vegetation in Taiwan was consistent with a warm tropical landscape. Thus there is no indication of dramatically reduced precipitation compared to modern. The relationship between precipitation amount and $\delta^{13}C$ is generally minimal for areas with annual precipitation more than 2000 mm/yr (Diefendorf and others, 2010), and as a result, it is unlikely that past changes in precipitation amount can account for observed changes in the sedimentary $\delta^{13}C_{n\text{-alkane}}$.

Catchment integration.— Plants that grow at high elevations are generally characterized by more positive $\delta^{13}C$ values than vegetation at lower elevations due to greater carboxylation efficiency at high altitudes (Körner and others, 1988). The positive correlation between elevation and plant $\delta^{13}C$ can be observed globally (Körner and others, 1988; Bird and others, 1994; Feakins and others, 2018), and empirical datasets show that an elevation difference of 3 km may translate to a carbon isotopic difference of ~2‰ (Körner and others, 1988). In a highly erosive mountain catchment, inputs from variable elevations can contribute to considerable spatial and temporal heterogeneity in organic $\delta^{13}C$ records within fluvial sediments. Changes in the hypsometry of vegetation produced throughout the Gaoping River catchment from LGM to recent could impart a temporal shift in the $\delta^{13}C$ of detrital organic matter. However, due to the relatively small magnitude of the carbon isotope change with elevation (Körner and others, 1988), LGM to Holocene changes in the mean elevation of organic matter deposited at both sites are unlikely to fully account for the observed temporal shift in carbon isotopes. However, differences in proximity to the orogen and catchment integration are likely to contribute to carbon isotope differences between onshore and offshore sedimentary records.

The onshore and offshore cores from the Gaoping River system have significant differences in the area-elevation distribution for the contributing catchment (fig. 1B). The offshore core integrates sediments delivered from a broad region in southwestern Taiwan, with half of the integrated area from coastal regions with elevations lower than 100 m. In contrast, the onshore core integrates predominately the Gaoping River catchment, with over 50% of the catchment area at an elevation higher than 1000 m. The high elevations and relief of the Taiwan orogen result in significant climate and ecosystem gradients over a short distance (Ri and Miura, 1993; Nagamatsu and Miura, 1997). In addition, during the last glacial, portions of the modern Gaoping River catchment may have been above treeline. Spatial differences in proximity to the orogen may result in greater variability in sediment geochemistry for sites proximal to the orogen in comparison to distal sites. This spatial dependence on the geochemical signature of sedimentary biomarkers may explain why the $\delta^{13}C_{n\text{-alkane}}$ records in the offshore core (which are significantly biased by low elevation organic source areas) show carbon isotope changes relating to atmospheric pCO_2 and $\delta^{13}C_{atm}$, while the onshore record is strongly biased by a combination of biologic and physical processes that affect $\delta^{13}C$ values.

LEAF-WAX HYDROGEN ISOTOPES

To the first order, $\delta^2H_{n\text{-alkane}}$ reflects the hydrogen isotope composition of the ambient water utilized by plants and modified by secondary factors such as species-specific biosynthetic factors, differences in water use efficiency/evapotranspiration, and soil or groundwater sourcing (Sachse and others, 2012). Thus, biomarker δ^2H is commonly used as a record of precipitation δ^2H. However, environmental factors such as variations in the ecosystem, climate, or topography and sediment source can all affect the $\delta^2H_{n\text{-alkane}}$ recorded in sedimentary archives. There are two key observations from our onshore and offshore biomarker hydrogen isotope records. The first is that $\delta^2H_{n\text{-alkane}}$ records from onshore and offshore sedimentary cores show a similar 10 to 15‰ positive temporal shift through the glacial-interglacial transition. The second is that the $\delta^2H_{n\text{-alkane}}$ record of onshore sediments (nC_{29}) is ~15 to 20‰ more negative than the offshore core. Here, we discuss potential environmental factors that affect temporal and spatial variation in the $\delta^2H_{n\text{-alkane}}$ records in southwestern Taiwan.

Vegetation.—A growing body of literature shows large isotopic differences in $\delta^2H_{n\text{-alkane}}$ across plant functional types (for example, Feakins and Sessions, 2010; Sachse and others, 2012; Oakes and others, 2016; Eley and others, 2018). In contrast to $\delta^{13}C_{n\text{-alkane}}$, $\delta^2H_{n\text{-alkane}}$ is not a diagnostic discriminator for C_3 and C_4 plants (Bi and others, 2005; Chikaraishi and Naraoka, 2007). However, leaf-wax biomarkers from different growth forms are commonly characterized by distinct isotopic fractionations. For example, grasses (graminoid) and herbs are shown to be more isotopically depleted in deuterium than trees and shrubs (Sachse and others, 2012; Oakes and others, 2016). Variations in the proportion of *n*-alkane inputs from trees/shrubs relative to grasses and herbs could produce observable shifts in the sedimentary biomarker δ^2H records. Specifically, a temporal shift in the proportion of grass-derived normal alkanes within a sedimentary pool would produce a more negative sedimentary $\delta^2H_{n\text{-alkane}}$ value than one produced under similar environmental conditions but with a higher proportion of trees/shrub-derived alkanes.

To examine the potential influences of vegetation changes on the $\delta^2H_{n\text{-alkane}}$, we compare *n*-alkane δ^2H records with pollen data from central and southern Taiwan. Records from the Toushe peat bog core in central Taiwan show that grasses comprise more than 40% of pollen preserved within the peat during the LGM. Grass pollen abundance reaches a low of ~10% during the late glacial period and then becomes high again during the Holocene (Liew and others, 2006) (fig. 4C). At Tongyoun Lake, the percentage of grass pollen reaches 40% during the LGM and decreases to around 20% in the Holocene (Lee and Liew, 2010). These two Taiwan sedimentary records reflect the same gradual warming and wetter climate of the last glacial-interglacial transition (Liew and others, 2006; Lee and Liew, 2010; Li and others, 2013) but show distinct, and at times, opposite patterns of grass abundance. These data indicate that local records may be readily biased by the immediate local ecosystem and sourcing of organic matter.

In Taiwan, although the pollen records show a progressive shift in vegetation proportions through the glacial-interglacial transition (Liew and others, 2006; Lee and Liew, 2010), the timing of shift is inconsistent with the timing of the shift in $\delta^2H_{n\text{-alkane}}$ of our records (fig. 4C). This discrepancy indicates that vegetation changes in Taiwan through the glacial-interglacial transition do not represent a fundamental vegetation turnover that is likely to change isotope fractionation at an ecosystem level. Offshore

$\delta^{13}C_{n\text{-alkane}}$ data show only minor (~1‰) variation from the last glacial to interglacial period, suggesting minimal to no change in C_3/C_4 inputs to sedimentary alkanes during the glacial-interglacial transition (fig. 3A). Therefore, we suggest that observed temporal increase in our $\delta^2H_{n\text{-alkane}}$ records are not strictly controlled by vegetation changes and predominantly reflect changing precipitation δ^2H during this period due to other environmental factors.

Precipitation amount.—In tropical regions, the "amount effect" is often invoked to interpret variability in the isotopic composition of past precipitation (Dansgaard, 1964). This is based on modern observations that the isotopic composition of precipitation is negatively correlated with precipitation amount due to greater removal of moisture from clouds during convective precipitation (Rozanski and others, 1993; Risi and others, 2008; McFarlin and others, 2019). In eastern Asia, stable isotopic records of paleoprecipitation are argued to be closely tied to changes in ancient precipitation amount. For example, cave stalagmite isotope ($\delta^{18}O_{stalagmite}$) records in China show a negative shift from the glacial to interglacial period, which is interpreted to reflect a decrease in precipitation $\delta^{18}O$ since the LGM (Wang and others, 2001; Dykoski and others, 2005) (fig. 4D). Multiple records from across the South East Asia region show an increase in precipitation from the glacial to the interglacial period (An and others, 2000; Liu and others, 2014; Chen and others, 2015). Proxy records that show a negative shift in precipitation isotope composition through deglaciation are interpreted to reflect increased rainfall intensity and changes in relative contribution from different moisture sources (Maher and Thompson, 2012; Liu and others, 2014).

Sedimentary records from the Taiwan region show an increase in precipitation amount from the glacial to the interglacial period (Yang and others, 2011; Yu and others, 2017). Increased convective precipitation from the LGM to the Holocene should translate to a negative shift in water isotopes due to the "amount effect" processes. This expectation for increased precipitation and decreased δ^2H water values are opposite to the observed trend in our $\delta^2H_{n\text{-alkane}}$ data. In both onshore and offshore cores, we observe a positive temporal shift in $\delta^2H_{n\text{-alkane}}$ from glacial to interglacial. This observation is opposite the expected change for an increase in large-scale convective precipitation and also opposite the isotope pattern observed in East Asian records of LGM to recent isotope hydrology (fig. 5). It is unlikely that the observed positive temporal shift in $\delta^2H_{n\text{-alkane}}$ in southwestern Taiwan provides a simple record of changes in precipitation amount and monsoon intensity. Factors other than precipitation amount such as regional temperature or sediment source altitude provide the best explanation of the long-term record of $\delta^2H_{n\text{-alkane}}$ in the Gaoping River catchment.

Regional temperature change and climate model results.—Global precipitation isotope data show a positive correlation with temperature (Dansgaard, 1964; Rozanski and others, 1993). This global temperature-isotope relationship is the result of planetary-scale distillation during heat and vapor transport from equatorial to polar regions. In mid- to high-latitude areas, temperature exerts a primary control on the distribution of stable isotopes in precipitation. However, in tropical regions, this relationship is complicated by "amount effect" considerations. Onshore and offshore $\delta^2H_{n\text{-alkane}}$ records from the Gaoping system show a positive isotope shift coincident with post-glacial high-latitude warming (Jouzel and others, 2007) (fig. 4E) and a 3 to 5°C warming of the South China Sea (He and others, 2008; Steinke and others, 2010, 2011) (fig. 4F). These data strongly suggest that the observed change in $\delta^2H_{n\text{-alkane}}$ from the LGM to present in Taiwan is associated with a temperature-driven change in the vapor source area and composition, rather than strictly due to changes in convective precipitation intensity.

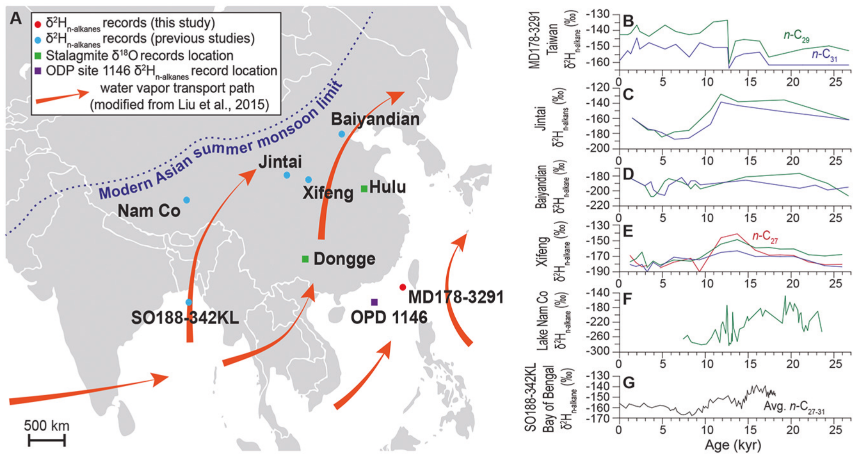

Fig. 5. (A) Schematic map of the water vapor transport path of Asian Summer Monsoon from the Indian Ocean and the Pacific Oceans (modified from Liu and others, 2015). The figure shows the comparison between (B) our offshore $\delta^2H_{n\text{-alkane}}$ records in Taiwan and existing $\delta^2H_{n\text{-alkane}}$ records across the Asian monsoon region: (C) Jintai (Li and others, 2018), (D) Baiyandian (Li and others, 2018), (E) Xifeng (Liu and Huang, 2015), (F) Lake Nam Co (Günther and others, 2015), (G) site SO188-342Kl in Bay of Bengal (Contreras-Rosales and others, 2014). The $\delta^2H_{n\text{-alkane}}$ record in OPD 1146 (purple square) covers 350-67 ka and does not cover the latest glacial-interglacial cycle. Stalagmite $\delta^{18}O$ records in Dongge and Hulu caves (green squares) can be found in fig. 4D.

Models of global precipitation isotopes (Lee and Fung, 2008; Steiger and others, 2017) predict an increase in water isotope composition (even in areas of the tropics) associated with the transition from glacial to interglacial conditions. To further test whether increases in $\delta^2H_{n\text{-alkane}}$ in Taiwan are consistent with expected shifts in isotope hydrology during the transition from last glacial to Holocene conditions, we conducted iCESM simulations for the SE Asia region. The iCESM climate modeling results for the LGM climate successfully reproduces the cooler and drier climate and the more negative precipitation δ^2H (δ^2H_p) during LGM in Taiwan (fig. 6). Simulated δ^2H_p during the LGM is around 12‰ more negative than PI (figs. 6A to 6C, table 2) and accounts for changes in water composition due to ice volume changes. This result matches the observed ~10 to 15‰ increase in $\delta^2H_{n\text{-alkane}}$ (uncorrected for ice volume effects) for both offshore and onshore cores from the glacial to interglacial period. These data strongly suggest that the observed change in $\delta^2H_{n\text{-alkane}}$ from the LGM to present in Taiwan is most consistent with the temperature-driven change in the vapor source area and composition, rather than strictly due to changes in convective precipitation intensity.

iCESM simulation results produced here disagree with proxy records from mainland Asia, which generally show isotopic enrichment of precipitation during the LGM. This disagreement may be due to the fact that climate models have difficulty simulating past isotopic responses in interior East Asia (Caley and others, 2014; Battisti and others, 2014; Tabor and others, 2018, 2020; Hu and others, 2019). Specifically, CESM may simulate too much moisture from the Pacific high and not enough moisture from India and the Bay of Bengal (Hu and others, 2019). Compared to China, India shows a more $\delta^{18}O$-rich signal in the LGM simulation relative to PI. Therefore, more Indian moisture transport into China at the LGM would lead to enrichment in China. Indeed, model results show a pronounced gradient in

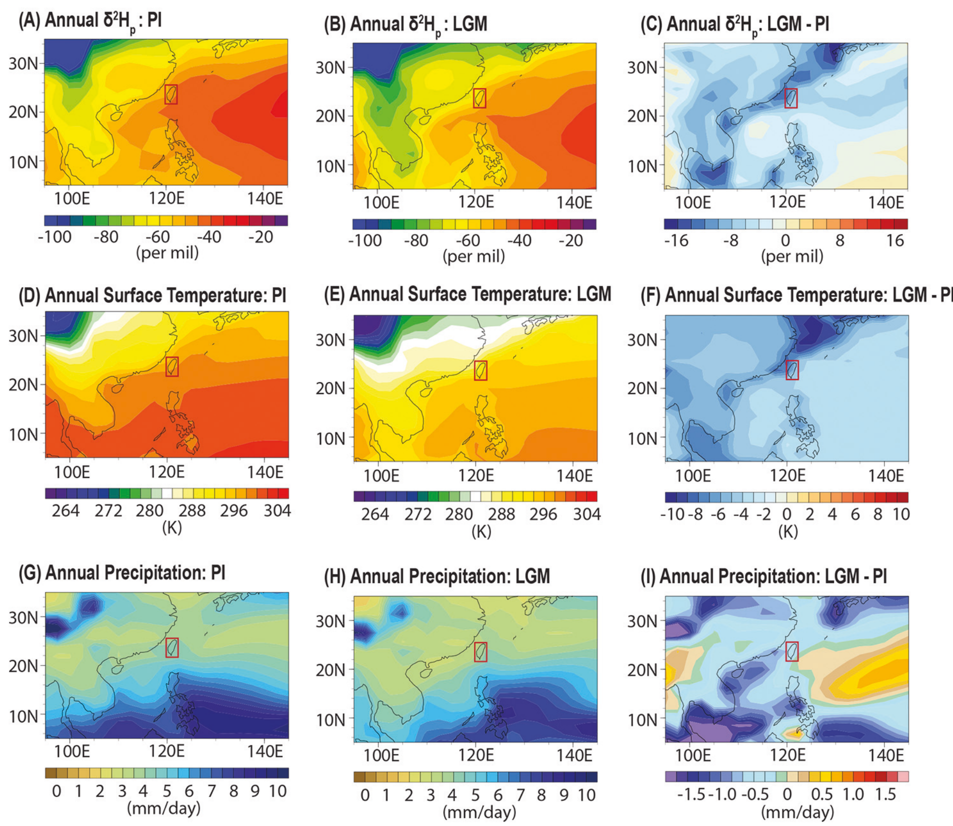

Fig. 6. iCESM simulation results for southeastern Asia. (A to C) Annual precipitation hydrogen isotope composition (δ^2H_p) during preindustrial (PI) and the Last Glacial Maximum (LGM) and the difference between LGM and PI; (D to F) mean annual surface temperature; (G to I) mean annual precipitation rate. The red squares represent the region where the average values in table 2 are calculated.

the δ^2H response at the edge of the plotted region in figure 6. If that region shifted further east, the model-proxy agreement would improve. Also, these simulations do not include dynamic vegetation, which might be important for the response in China (for example, Tabor and others, 2020).

Deglaciation and Isotope Hydrology in Asian Monsoon Region

Across East and South Asia, the Asian Summer Monsoon is the predominant factor controlling the spatial precipitation gradient. Asian Summer Monsoon moisture originates in the Indian Ocean and is transported across the Indochina Peninsula to eastern China, where it is affected by the Western Pacific Subtropical High, which is accompanied by strong southerly wind (fig. 5). As a result, the isotopic composition of precipitation in this region reflects the complex combination of the characteristics of the moisture sources, either an Indian-source or local Pacific-source, and distillation processes through the vapor transport (Maher and Thompson, 2012; Liu and others, 2014). Paleo precipitation isotope records from the Asian Monsoon regions are often interpreted as primarily reflecting the monsoon rainfall intensity, while signals from different locations might also be influenced by the distillation processes during moisture transport or local aridity

TABLE 2

The regional average iCESM simulation results during the Last Glacial Maximum (LGM) and Preindustrial (PI)

	Mean Annual δ^2Hp (‰)	Mean Annual Surface temperature (K)	Mean Annual Precipitation Rate (mm/day)
PI	-51.6 ± 7.31	296.5 ± 0.37	4.14 ± 0.782
LGM	-64.3 ± 7.21	288.7 ± 0.44	3.43 ± 0.596
LGM-PI	-12.7 ± 7.26	-7.8 ± 0.40	-0.71 ± 0.690

response to climate change (Wang and others, 2001; Dykoski and others, 2005; Liu and Huang, 2005; Contreras-Rosales and others, 2014; Günther and others, 2015; Li and others, 2018).

$\delta^2H_{n\text{-alkane}}$ records from onshore and offshore localities of SW Taiwan show a positive shift during the last glacial-interglacial transition. This isotopic change is opposite $\delta^{18}O_{stalagmite}$ records in China and other isotopic records from the Bay of Bengal (Dykoski and others, 2005) (figs. 4 and 5) (Contreras-Rosales and others, 2014) (fig. 5) but is not unique for the SE Asian region. For example, Thomas and others (2014) show that long-term glacial-interglacial variations in $\delta^2H_{n\text{-alkane}}$ have a systematic phase difference from records in central China. Their record of glacial-interglacial $\delta^2H_{n\text{-alkane}}$ matches the pattern observed in records from SW Taiwan presented here. They suggest that $\delta^2H_{n\text{-alkane}}$ in southeast China is strongly controlled by temperature, whereas $\delta^{18}O_{stalagmite}$ records from central China are more strongly influenced by global ice volume changes. Spatial differences in isotopic response between glacial and interglacial time periods may result from changes in the mid-latitude westerlies, which drive more isotopically enriched Pacific moisture eastward during the interglacial, and thus less enriched Pacific moisture reaches inland Asia.

An alternative explanation for spatial differences in LGM to recent paleo precipitation isotope records between continental Asia and the South China Sea is that the source of moisture is different for these two areas. The isotopic composition of precipitation in the interior of the Asian continent reflects upstream monsoon regions, including the Indian Ocean (Liu and others, 2014; Maher and Thompson, 2012; Tabor and others, 2018; Hu and others, 2019). In contrast, precipitation across the South China Sea may reflect greater contributions of locally derived and Pacific moisture (Hu and others, 2019). The contrast between new biomarker hydrogen isotope data presented here and paleo precipitation isotope records from mainland Asia points to the complex heterogeneity of precipitation records and hydrological responses to deglaciation and changing orbital parameters in this region.

Catchment Integration and Biomarker Isotopes

The stable isotopic composition of precipitation is shown to be related to the height of topography due to Rayleigh distillation during progressive rainout when moist airmasses encounter a topographic barrier (Dansgaard, 1964). As airmasses lift and cool, moisture is progressively removed through precipitation, generating a characteristic Rayleigh distillation pattern in the isotope data. Precipitation that falls higher in a catchment (Dansgaard, 1964; Poage and Chamberlain, 2001; Rowley and

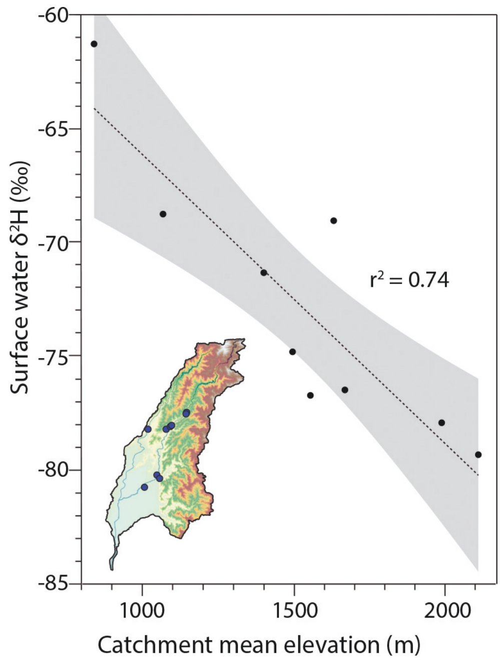

Fig. 7. The relationship between catchment mean elevation and surface water δ2H for the Gaoping River catchment. The gray area represents the 95% confidence interval.

others, 2001; Hren and others, 2010) is generally characterized by more negative isotope compositions. We collected and measured nine water samples from the Gaoping River to examine how surface water isotopic composition varies with elevation in this region (fig. 7; table 3). These data show an isotope-elevation relationship characterized by an ~15‰ decrease in δ^2H per km elevation, which overlaps with data from a global compilation that shows a change in precipitation δ^2H of ~15 to 20‰ per km of elevation in tropical regions (Poage and Chamberlain, 2001).

The Gaoping River catchment spans ~4 km of elevation, with expected precipitation and biomarker isotopic variation of nearly 60 to 80‰ from coast to the peak. The isotope composition of the terrestrial leaf-wax biomolecules preserved in sediments records the isotope composition of organic matter produced within the catchment. $\delta^2H_{n\text{-}C29}$ of both onshore and offshore cores record an ~10 to 15‰ positive shift during the last deglaciation (fig. 8). Consistency between these records and isotope-enabled global climate simulations shows that isotopic signals preserved in both sites are strongly controlled by shifts in isotope hydrology related to regional post-glacial warming. However, onshore $\delta^2H_{n\text{-}C29}$ values are 15 to 20‰ more negative than those preserved in the offshore core (fig. 8). This difference most likely reflects differences in sediment source because distal locations have a larger integrated catchment and lower average catchment elevation than locations proximal to the orogen. The onshore core site is characterized by a mean catchment elevation of ~1100 m, whereas the offshore site has a mean catchment elevation of ~500 m. Moreover, in the Gaoping submarine canyon, submarine transport processes such as sediment remobilization by waves, contributions from sediment plumes of nearby small rivers, or suspension of sediments by ocean currents could contribute sediments and organic material from a wider area (Liu and others, 2002; Liu and Lin, 2004) which would produce an even lower integrated source

TABLE 3

δ^2H results of modern river water of the Gaoping river catchment

Sample	Longitude	Latitude	Locality elevation (m)	Catchment mean elevation (m)	River water δ^2H (‰)
TW17-GP01	120.593	23.094	260	1499	-71
TW17-GP02	120.679	23.094	419	843	-58
TW17-GP03	120.699	23.106	376	1635	-66
TW17-GP04	120.706	23.111	387	1991	-74
TW17-GP05	120.777	23.169	561	1071	-65
TW17-GP06	120.774	23.162	521	2113	-75
TW17-GP07	120.636	22.892	145	1672	-73
TW17-GP08	120.649	22.877	144	1404	-68
TW17-GP09	120.577	22.838	65	1558	-73

elevation. Based on modern isotope-elevation lapse rates for Taiwan waters, one might expect a biomarker δ^2H difference of 9 to 12‰ between onshore and offshore deposits. However, the magnitude of isotopic difference in $\delta^2H_{n\text{-alkane}}$ exceeds that predicted from water isotope data alone. This indicates that the sediments and organic materials are not delivered homogeneously throughout the catchment, and other processes likely contribute to differences in integrated biomarker isotope signal.

Numerous studies demonstrate that the primary sediment production mechanism in Taiwan is through the frequent landslides that occur across this tectonically active and rapidly eroding landscape (Dadson and others, 2003, 2004; Hilton and others, 2008, 2011, 2012; Zhang and others, 2018). Because of the tropical climate and high precipitation, primary production is generally high at nearly all elevations of the major river catchments. As a result, the integrated source elevation of organic matter that is recorded by $\delta^2H_{n\text{-alkane}}$ may reflect the mean elevation of the landslide-occurring area throughout the catchment. The spatial distribution of landslides across the hillslope is affected by the triggering mechanisms: landslides triggered by intense rainfall tend to occur at lower elevation hillslopes (Montgomery and Dietrich, 1994; Densmore and Hovius, 2000), while earthquake-induced landslides may occur more frequently in higher-elevation, steep topography (Densmore and Hovius, 2000; Larsen and Montgomery, 2012; Wang and others, 2020).

Previous studies show that since the last glacial period to present, there has been an increase in landslide frequency, organic matter delivery, and submarine turbidity currents in Taiwan due to strengthened monsoon intensity and precipitation (Hsieh and Chyi, 2010; Yang and others, 2011; Yu and others, 2017). Nevertheless, the 15 to 20‰ difference in $\delta^2H_{n\text{-alkane}}$ between onshore and offshore cores remain the same in either the glacial period or interglacial period. This implies that any climate-induced changes to landslide frequency or area are not clearly manifested in the biomarker isotope record here. In addition, while climate feedbacks to erosion have the potential to bias interpretations of detrital organic biomarker isotopes records, the temperature change associated with the LGM to recent transition is one of the largest climate shifts of the past several million years. Our results show that the $\delta^2H_{n\text{-alkane}}$ variation during this extreme climate transition is only around 10 to 15‰. This suggests that in a tectonically-

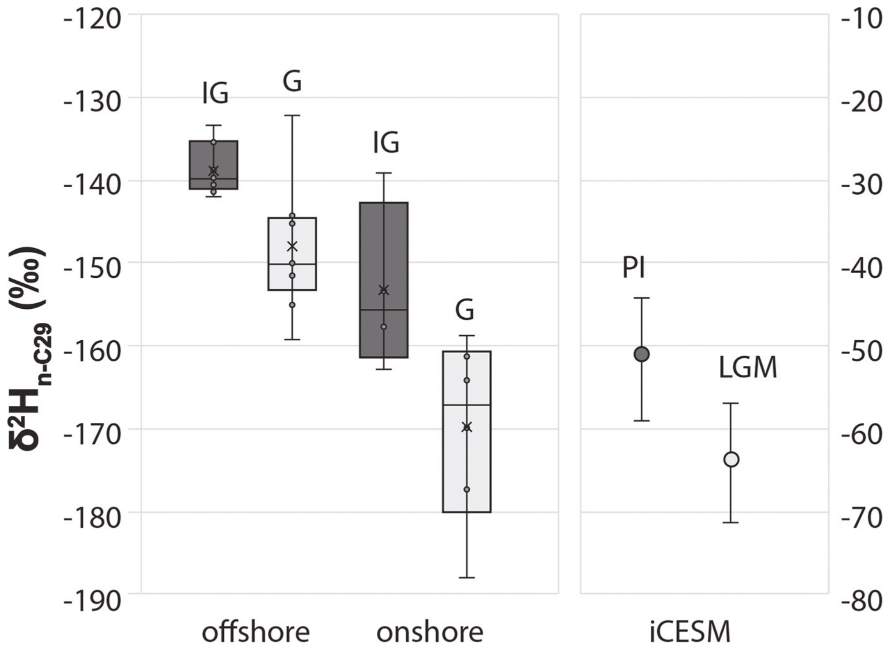

Fig. 8. Comparison between offshore core (MD178-3291) and onshore core(Chaoliao) $\delta^2H_{n\text{-}C29}$ and iCESM simulated precipitation δ^2H of glacial (G, light gray) and interglacial (IG, dark gray) periods, and the iCESM simulation results of precipitation δ^2H during glacial (Last Glacial Maximum, LGM, light gray) and interglacial (preindustrial, PI, dark gray) periods. Both cores show a 10 to 15‰ positive temporal shift in $\delta^2H_{n\text{-}C29}$ from glacial to interglacial, which agrees with the iCESM results. The onshore $\delta^2H_{n\text{-}C29}$ records are 15 to 20‰ smaller than the offshore core, indicating the influences of catchment integration processes.

active tropical mountain system such as Taiwan, isotopic variations in sedimentary records spanning the past several million years will most strongly reflect changes to catchment integration of sediments and organic materials.

CONCLUSION

We analyzed the stable hydrogen and carbon isotopes of plant-derived normal alkanes preserved in onshore and offshore sediments of the Gaoping River-submarine canyon system in southwestern Taiwan to examine climatic and geomorphic influences on geochemical records in a tectonically-active tropical mountain system. These data produce two key results. First, the shift in $\delta^2H_{n\text{-alkane}}$ and $\delta^{13}C_{n\text{-alkane}}$ since LGM in southwestern Taiwan is best explained by regional warming and increased atmospheric pCO_2 during the last deglaciation. $\delta^2H_{n\text{-alkane}}$ in both onshore and offshore sediments record a 10 to 15‰ positive shift from the LGM to recent. This pattern is opposite records of South and East Asia but is consistent with the results of a new iCESM simulation of climate and isotope hydrology across this region. This suggests that regional temperature plays a key role in shaping isotope hydrology and biomarker $\delta^2H_{n\text{-alkane}}$ in Taiwan. Second, there is a clear offset in biomarker hydrogen isotope composition for organic compounds preserved in offshore and onshore sediments of the same catchment system. Specifically, onshore sediments have $\delta^2H_{n\text{-}C29}$ 15 to 20‰ more negative than those preserved in offshore settings. This offset is likely due to differences in the integration of sediments and organic matter throughout the catchment. Depositional sites closer to the orogen are characterized by higher mean catchment elevations and thus more depleted in isotopic signatures of the organic molecules produced in a smaller integrated catchment. This offset did not vary through the glacial-interglacial transition, indicating that climate change may have affected erosion rate and the amount of sediments produced, but not erosion provenance and catchment integration. In total, these data highlight the critical role that depositional setting plays in controlling organic molecular stable isotope records of paleoenvironments and must be taken into consideration in paleoenvironmental reconstruction.

ACKNOWLEDGMENTS

We thank Nemiah Ladd, Zhonghui Liu, and Guangsheng Zhuang for helpful comments that improved this manuscript. This work was supported in part by the US National Science Foundation (EAR-1752815 and EAR-1650396). Tabor acknowledges funding from the National Science Foundation AGS-1804747. The CESM project is supported primarily by the NSF. This material is based upon work supported by the National Center for Atmospheric Research, which is a major facility sponsored by the NSF under Cooperative Agreement No. 1852977. Computing and data storage resources, including the Cheyenne supercomputer (doi:10.5065/D6RX99HX), were provided by the Computational and Information Systems Laboratory (CISL) at NCAR.

REFERENCES

An, Z., Porter, S. C., Kutzbach, J. E., Xihao, W., Suming, W., Xiaodong, L., Xiaoqiang, L., and Weijian, Z., 2000, Asynchronous Holocene optimum of the East Asian monsoon: Quaternary Science Reviews, v. 19, n. 8, p. 743–762, https:10.1016/S0277-3791(99)00031-1

Battisti, D. S., Ding, Q., and Roe, G. H., 2014, Coherent pan-Asian climatic and isotopic response to orbital forcing of tropical insolation: Journal of Geophysical Research: Atmospheres, v. 119, n. 21, p. 11,997–12,020, https:10.1002/2014JD021960

Beerling, D., 1996, ^{13}C discrimination by fossil leaves during the late-glacial climate oscillation 12-10 ka BP: Measurements and physiological controls: Oecologia, v. 108, n. 1, p. 29–37, https:10.1007/BF00333211

Beerling, D. J., and Royer, D. L., 2002, Fossil plants as indicators of the Phanerozoic global carbon cycle: Annual Review of Earth and Planetary Sciences, v. 30, n. 1, p. 527–556, https:10.1146/annurev.earth.30.091201.141413

Bi, X., Sheng, G., Liu, X., Li, C., and Fu, J., 2005, Molecular and carbon and hydrogen isotopic composition of *n*-alkanes in plant leaf waxes: Organic Geochemistry, v. 36, n. 10, p. 1405–1417, https:10.1016/j.orggeochem.2005.06.001

Bird, M. I., Haberle, S. G., and Chivas, A. R., 1994, Effect of altitude on the carbon-isotope composition of forest and grassland soils from Papua New Guinea: Global Biogeochemical Cycles, v. 8, n. 1, p. 13–22, https:10.1029/93GB03487

Bliedtner, M., von Suchodoletz, H., Schäfer, I., Welte, C., Salazar, G., Haas, M., Dubois, N., and Zech, R., 2020, Age and origin of leaf wax *n*-Alkanes in fluvial sediment-paleosol sequences and implications for paleoenvironmental reconstructions: Hydrology and Earth System Sciences, v. 24, n. 4, p. 2105–2120, https://doi.org/10.5194/hess-24-2105-2020

Blum, M. D., and Törnqvist, T. E., 2000, Fluvial responses to climate and sea-level change: A review and look forward: Sedimentology, v. 47, n. s1, p. 2–48, https://doi.org/10.1046/j.1365-3091.2000.00008.x

Bowling, D. R., McDowell, N. G., Bond, B. J., Law, B. E., and Ehleringer, J. R., 2002, ^{13}C content of ecosystem respiration is linked to precipitation and vapor pressure deficit: Oecologia, v. 131, n. 1, p. 113–124, https:10.1007/s00442-001-0851-y

Braconnot, P., Harrison, S. P., Kageyama, M., Bartlein, P. J., Masson-Delmotte, V., Abe-Ouchi, A., Otto-Bliesner, B., and Zhao, Y., 2012, Evaluation of climate models using palaeoclimatic data: Nature Climate Change, v. 2, n. 6, p. 417–424, https:10.1038/nclimate1456

Brittingham, A., Hren, M. T., and Hartman, G., 2017, Microbial alteration of the hydrogen and carbon isotopic composition of *n*-alkanes in sediments: Organic Geochemistry, v. 107, p. 1–8, https:10.1016/j.orggeochem.2017.01.010

Bush, R. T., and McInerney, F. A., 2013, Leaf wax *n*-alkane distributions in and across modern plants: Implications for paleoecology and chemotaxonomy: Geochimica et Cosmochimica Acta, v. 117, p. 161–179, https:10.1016/j.gca.2013.04.016

Caley, T., Roche, D. M., and Renssen, H., 2014, Orbital Asian summer monsoon dynamics revealed using an isotope-enabled global climate model: Nature Communications, v. 5, n. 1, p. 1–6, https:10.1038/ncomms6371

Chen, F., Xu, Q., Chen, J., Birks, H. J., Liu, J., Zhang, S., Jin, L., An, C., Telford, R. J., Cao, X., Wang, Z., Zhang, X., Selvaraj, K., Lu, H., Li, Y., Zheng, Z., Wang, H., Zhou, A., Dong, G., Zhang, J., Huang, X., Bloemendal, J., and Rao, Z., 2015, East Asian summer monsoon precipitation variability since the last deglaciation: Scientific Reports, v. 5, p. 11186, https:10.1038/srep11186

Chen, Y. G., 1998, Taiwan ground water observation net project, Phase I annual report: Age constrain and stratigraphy correlation (in Chinese): Taiwan Bureau of Energy Publication, 60 p.

Chen, Y. G., and Liu, T. K., 1996, Sea Level Changes in the Last Several Thousand Years, Penghu Islands, Taiwan Strait: Quaternary Research, v. 45, n. 3, p. 254–262, https:10.1006/qres.1996.0026

Chiang, C. S., and Yu, H. S., 2006, Morphotectonics and incision of the Kaoping submarine canyon, SW Taiwan orogenic wedge: Geomorphology, v. 80, n. 3–4, p. 199–213, https:10.1016/j.geomorph.2006.02.008

———, 2008, Evidence of hyperpycnal flows at the head of the meandering Kaoping Canyon off SW Taiwan: Geo-Marine Letters, v. 28, n. 3, p. 161–169, https:10.1007/s00367-007-0098-7

Chikaraishi, Y., and Naraoka, H., 2003, Compound-specific δD–$\delta^{13}C$ analyses of *n*-alkanes extracted from terrestrial and aquatic plants: Phytochemistry, v. 63, n. 3, p. 361–371, https:10.1016/S0031-9422(02)00749-5

———, 2007, $\delta^{13}C$ and δD relationships among three *n*-alkyl compound classes (*n*-alkanoic acid, *n*-alkane and *n*-alkanol) of terrestrial higher plants: Organic Geochemistry, v. 38, n. 2, p. 198–215, https:10.1016/j.orggeochem.2006.10.003

Contreras-Rosales, L. A., Jennerjahn, T., Tharammal, T., Meyer, V., Lückge, A., Paul, A., and Schefuß, E., 2014, Evolution of the Indian Summer Monsoon and terrestrial vegetation in the Bengal region during the past 18 ka: Quaternary Science Reviews, v. 102, p. 133–148, https:10.1016/j.quascirev.2014.08.010

Dadson, S. J., Hovius, N., Chen, H. G., Dade, W. B., Hsieh, M. L., Willett, S. D., Hu, J. C., Horng, M. J., Chen, M. C., Stark, C. P., Lague, D., and Lin, J. C., 2003, Links between erosion, runoff variability and seismicity in the Taiwan orogen: Nature, v. 426, n. 6967, p. 648–651, https:10.1038/nature02150

Dadson, S. J., Hovius, N., Chen, H., Dade, W. B., Lin, J. C., Hsu, M. L., Lin, C. W., Horng, M. J., Chen, T. C., Milliman, J., and Stark, C. P., 2004, Earthquake-triggered increase in sediment delivery from an active mountain belt: Geology, v. 32, n. 8, p. 733–736, https:10.1130/G20639.1

Dansgaard, W., 1964, Stable isotopes in precipitation: Tellus, v. 16, n. 4, p. 436–468, https:10.3402/tellusa.v16i4.8993

Densmore, A. L., and Hovius, N., 2000, Topographic fingerprints of bedrock landslides: Geology, v. 28, n. 4, p. 371–374, https://doi.org/10.1130/0091-7613(2000)28<371:TFOBL>2.0.CO;2

Diefendorf, A. F., and Freimuth, E. J., 2017, Extracting the most from terrestrial plant-derived *n*-alkyl lipids and their carbon isotopes from the sedimentary record: A review: Organic Geochemistry, v. 103, p. 1–21, https:10.1016/j.orggeochem.2016.10.016

Diefendorf, A. F., Mueller, K. E., Wing, S. L., Koch, P. L., and Freeman, K. H., 2010, Global patterns in leaf ^{13}C discrimination and implications for studies of past and future climate: Proceedings of the National Academy of Sciences of the United States of America, v. 107, n. 13, p. 5738–5743, https:10.1073/pnas.0910513107

Duplessy, J.-C., Labeyrie, L., and Waelbroeck, C., 2002, Constraints on the ocean oxygen isotopic enrichment between the Last Glacial Maximum and the Holocene: Paleoceanographic implications: Quaternary Science Reviews, v. 21, n. 1–3, p. 315–330, https://doi.org/10.1016/S0277-3791(01)00107-X

Dykoski, C. A., Edwards, R. L., Cheng, H., Yuan, D., Cai, Y., Zhang, M., Lin, Y., Qing, J., An, Z., and Revenaugh, J., 2005, A high-resolution, absolute-dated Holocene and deglacial Asian monsoon record from Dongge Cave, China: Earth and Planetary Science Letters, v. 233, n. 1–2, p. 71–86, https:10.1016/j.epsl.2005.01.036

Eglinton, G., and Hamilton, R. J., 1967, Leaf Epicuticular Waxes: Science, v. 156, n. 3780, p. 1322–1335, https:10.1126/science.156.3780.1322

Eglinton, T. I., Galy, V. V., Hemingway, J. D., Feng, X., Bao, H., Blattmann, T. M., Dickens, A. F., Gies, H., Giosan, L., Haghipour, N., Hou, P., Lupker, M., McIntyre, C. P., Montluçon, D. B., Peucker-Ehrenbrink, B., Ponton, C., Schefuß, E., Schwab , M. S., Voss, B. M., Wacker, L., Wu, Y., and Zhao, M., 2021, Climate control on terrestrial biospheric carbon turnover: Proceedings of the National Academy of Sciences of the United States of America, v. 118, n. 8, https://doi.org/10.1073/pnas.2011585118

Ehleringer, J. R., and Cerling, T. E., 1995, Atmospheric CO_2 and the ratio of intercellular to ambient CO_2 concentrations in plants: Tree Physiology, v. 15, n. 2, p. 105–111, https://doi.org/10.1093/treephys/15.2.

Eley, Y. L., and Hren, M. T., 2018, Reconstructing vapor pressure deficit from leaf wax lipid molecular distributions: Scientific Reports, v. 8, p. 1–8, https:10.1038/s41598-018-21959-w

Eley, Y., Dawson, L., Black, S., Andrews, J., and Pedentchouk, N., 2014, Understanding $^2H/^1H$ systematics of leaf wax *n*-alkanes in coastal plants at Stiffkey saltmarsh, Norfolk, UK: Geochimica et Cosmochimica Acta, v. 128, p. 13–28, https:10.1016/j.gca.2013.11.045

Eley, Y., Dawson, L., and Pedentchouk, N., 2016, Investigating the carbon isotope composition and leaf wax *n*-alkane concentration of C_3 and C_4 plants in Stiffkey saltmarsh, Norfolk, UK: Organic Geochemistry, v. 96, p. 28–42, https:10.1016/j.orggeochem.2016.03.005

Eley, Y., White, J., Dawson, L., Hren, M., and Pedentchouk, N., 2018, Variation in hydrogen isotope composition among salt marsh plant organic compounds highlights biochemical mechanisms controlling biosynthetic fractionation: Journal of Geophysical Research: Biogeosciences, v. 123, n. 9, p. 2645–2660, https:10.1029/2018JG004403

Elsig, J., Schmitt, J., Leuenberger, D., Schneider, R., Eyer, M., Leuenberger, M., Joos, F., Fischer, H., and Stocker, T. F., 2009, Stable isotope constraints on Holocene carbon cycle changes from an Antarctic ice core: Nature, v. 461, n. 7263, p. 507–510, https:10.1038/nature08393

Farquhar, G. D., and Sharkey, T. D., 1982, Stomatal conductance and photosynthesis: Annual Review of Plant Physiology, v. 33, n. 1, p. 317–345, https:10.1146/annurev.pp.33.060182.001533
Farquhar, G. D., Ehleringer, J. R., and Hubick, K. T., 1989, Carbon isotope discrimination and photosynthesis: Annual review of Plant Physiology and Plant Molecular Biology, v. 40, n. 1, p. 503–537, https:10.1146/annurev.pp.40.060189.002443
Feakins, S. J., and Sessions, A. L., 2010, Controls on the D/H ratios of plant leaf waxes in an arid ecosystem: Geochimica et Cosmochimica Acta, v. 74, n. 7, p. 2128–2141, https:10.1016/j.gca.2010.01.016
Feakins, S. J., Wu, M. S., Ponton, C., Galy, V., and West, A. J., 2018, Dual isotope evidence for sedimentary integration of plant wax biomarkers across an Andes-Amazon elevation transect: Geochimica et Cosmochimica Acta, v. 242, p. 64–81, https:10.1016/j.gca.2018.09.007
Fellin, M. G., Chen, C. Y., Willett, S. D., Christl, M., and Chen, Y.-G., 2017, Erosion rates across space and timescales from a multi-proxy study of rivers of eastern Taiwan: Global and Planetary Change, v. 157, p. 174–193, https:10.1016/j.gloplacha.2017.07.012
Fornace, K. L., Whitney, B. S., Galy, V., Hughen, K. A., and Mayle, F. E., 2016, Late Quaternary environmental change in the interior South American tropics: New insight from leaf wax stable isotopes: Earth and Planetary Science Letters, v. 438, p. 75–85, https:10.1016/j.epsl.2016.01.007
Galy, V., Eglinton, T., France-Lanord, C., and Sylva, S., 2011, The provenance of vegetation and environmental signatures encoded in vascular plant biomarkers carried by the Ganges–Brahmaputra rivers: Earth and Planetary Science Letters, v. 304, n. 1–2, p. 1–12, https:10.1016/j.epsl.2011.02.003
Garcin, Y., Schefuß, E., Schwab, V. F., Garreta, V., Gleixner, G., Vincens, A., Todou, G., Séné, O., Onana, J. M., Achoundong, G., and Sachse, D., 2014, Reconstructing C_3 and C_4 vegetation cover using *n*-alkane carbon isotope ratios in recent lake sediments from Cameroon, Western Central Africa: Geochimica et Cosmochimica Acta, v. 142, p. 482–500, https:10.1016/j.gca.2014.07.004
Günther, F., Witt, R., Schouten, S., Mäusbacher, R., Daut, G., Zhu, L., Xu, B., Yao, T., and Gleixner, G., 2015, Quaternary ecological responses and impacts of the Indian Ocean Summer Monsoon at Nam Co, Southern Tibetan Plateau: Quaternary Science Reviews, v. 112, p. 66–77, https:10.1016/j.quascirev.2015.01.023
He, J., Zhao, M., Li, L., Wang, H., and Wang, P., 2008, Biomarker Evidence of Relatively Stable Community Structure in the Northern South China Sea during the Last Glacial and Holocene: Terrestrial, Atmospheric and Oceanic Sciences Journal, v. 19, n. 4, https:10.3319/TAO.2008.19.4.377(IMAGES)
Hilton, R. G., Galy, A., Hovius, N., Chen, M.-C., Horng, M.-J., and Chen, H., 2008, Tropical-cyclone-driven erosion of the terrestrial biosphere from mountains: Nature Geoscience, v. 1, n. 11, p. 759–762, https:10.1038/ngeo333
Hilton, R. G., Galy, A., Hovius, N., Horng, M. J., and Chen, H., 2011, Efficient transport of fossil organic carbon to the ocean by steep mountain rivers: An orogenic carbon sequestration mechanism: Geology, v. 39, n. 1, p. 71–74, https:10.1130/G31352.1
Hilton, R. G., Galy, A., Hovius, N., Kao, S.-J., Horng, M.-J., and Chen, H., 2012, Climatic and geomorphic controls on the erosion of terrestrial biomass from subtropical mountain forest: Global Biogeochemical Cycles, v. 26, n. 3, p. GB3014, https://doi.org/10.1029/2012GB004314
Hren, M. T., Pagani, M., Erwin, D. M., and Brandon, M., 2010, Biomarker reconstruction of the early Eocene paleotopography and paleoclimate of the northern Sierra Nevada: Geology, v. 38, n. 1, p. 7–10, https://doi.org/10.1130/G30215.1
Hren, M. T., Eley, Y., White, J. D., Oakes, A., Wang, C., Smolen, J., and Truong, K, 2018, Examining leaf-wax signatures from biosynthesis to burial: A systems perspective on interpreting leaf wax records: 2018 AGU Fall Meeting Abstracts.
Hsieh, M. L., and Chyi, S. J., 2010, Late Quaternary mass-wasting records and formation of fan terraces in the Chen-yeo-lan and Lao-nung catchments, central-southern Taiwan: Quaternary Science Reviews, v. 29, n. 11–12, p. 1399–1418, https:10.1016/j.quascirev.2009.10.002
Hsu, F. H., Su, C. C., Wang, C. H., Lin, S., Liu, J., and Huh, C. A., 2014, Accumulation of terrestrial organic carbon on an active continental margin offshore southwestern Taiwan: Source-to-sink pathways of river-borne organic particles: Journal of Asian Earth Sciences, v. 91, p. 163–173, https:10.1016/j.jseaes.2014.05.006
Hsu, R. T., Liu, J. T., Su, C. C., Kao, S. J., Chen, S. N., Kuo, F. H., and Huang, J. C., 2014, On the links between a river's hyperpycnal plume and marine benthic nepheloid layer in the wake of a typhoon: Progress in Oceanography, v. 127, p. 62–73, https:10.1016/j.pocean.2014.06.001
Hu, J., Emile-Geay, J., Tabor, C., Nusbaumer, J., and Partin, J., 2019, Deciphering oxygen isotope records from Chinese speleothems with an isotope-enabled climate model: Paleoceanography and Paleoclimatology, v. 34, n. 12, p. 2098–2112, https:10.1029/2019PA003741
Hurrell, J. W., Holland, M. M., Gent, P. R., Ghan, S., Kay, J. E., Kushner, P. J., Lamarque, J.-F., Large, W. G., Lawrence, D., Lindsay, K., Lipscomb, W. H., Long, M. C., Mahowald, N., Marsh, D. R., Neale, R. B., Rasch, P., Vavrus, S., Vertenstein, M., Bader, D., Collins, W. D., Hack, J. J., Kiehl, J., and Marshall, S., 2013, The community earth system model: a framework for collaborative research: Bulletin of the American Meteorological Society, v. 94, n. 9, p. 1339–1360, https:10.1175/BAMS-D-12-00121.1
Jouzel, J., Masson-Delmotte, V., Cattani, O., Dreyfus, G., Falourd, S., Hoffmann, G., Minster, B., Nouet, J., Barnola, J.-M., Chappellaz, J., Fischer, H., Gallet, J. C., Johnsen, S., Leuenberger, M., Loulergue, L., Luethi, D., Oerter, H., Parrenin, F., Raisbeck, G., Raynaud, D., Schilt, A., Schwander, J., Selmo, E., Souchez, R., Spahni, R., Stauffer, B., Steffensen, J. P., Stenni, B., Stocker, T. F., Tison, J. L., Werner, M., and Wolff, E. W., 2007, Orbital and millennial Antarctic climate variability over the past 800,000 years: Science, v. 317, n. 5839, p. 793–796, https:10.1126/science.1141038

Kao, S. J., and Milliman, J. D., 2008, Water and Sediment Discharge from Small Mountainous Rivers, Taiwan: The Roles of Lithology, Episodic Events, and Human Activities: The Journal of Geology, v. 116, n. 5, p. 431–448, https:10.1086/590921

Kikuchi, T., and Miura, O., 1993, Vegetation patterns in relation to micro-scale landforms in hilly land regions: Vegetatio, v. 106, n. 2, p. 147–154, https://doi.org/10.1007/BF00045068

Körner, C., Farquhar, G. D., and Roksandic, Z., 1988, A global survey of carbon isotope discrimination in plants from high altitude: Oecologia, v. 74, p. 623–632, https:10.1007/BF00380063

Larsen, I. J., and Montgomery, D. R., 2012, Landslide erosion coupled to tectonics and river incision: Nature Geoscience, v. 5, n. 7, p. 468–473, https:10.1038/ngeo1479

Lee, C. Y., and Liew, P. M., 2010, Late Quaternary vegetation and climate changes inferred from a pollen record of Dongyuan Lake in southern Taiwan: Palaeogeography, Palaeoclimatology, Palaeoecology, v. 287, n. 1–4, p. 58–66, https:10.1016/j.palaeo.2010.01.015

Lee, J. E., and Fung, I., 2008, "Amount effect" of water isotopes and quantitative analysis of post-condensation processes: Hydrological Processes, v. 22, n. 1, p. 1–8, https:10.1002/hyp.6637

LeGrande, A. N., and Schmidt, G. A., 2006, Global gridded data set of the oxygen isotopic composition in seawater: Geophysical Research Letters, v. 33, n. 12, https:10.1029/2006GL026011

Li, H. C., Liew, P. M., Seki, O., Kuo, T. S., Kawamura, K., Wang, L. C., and Lee, T. Q., 2013, Paleoclimate variability in central Taiwan during the past 30 Kyrs reflected by pollen, $\delta^{13}C_{TOC}$, and n-alkane-δD records in a peat sequence from Toushe Basin: Journal of Asian Earth Sciences, v. 69, p. 166–176, https:10.1016/j.jseaes.2012.12.005

Li, Y., Yang, S., Xiao, J., Jiang, W., and Yang, X., 2018, Hydrogen isotope ratios of leaf wax *n*-alkanes in loess and floodplain deposits in northern China since the Last Glacial Maximum and their paleoclimatic significance: Palaeogeography, Palaeoclimatology, Palaeoecology, v. 509, p. 91–97, https:10.1016/j.palaeo.2017.08.009

Liew, P. M., 1998, Taiwan ground water observation net project Phase I annual report: Pollen records and stratigraphy correlation analysis of Pintong Plain, Taiwan (in Chinese): Taiwan Bureau of Energy Publication, 39 p.

Liew, P. M., Huang, S. Y., and Kuo, C. M., 2006, Pollen stratigraphy, vegetation and environment of the last glacial and Holocene—A record from Toushe Basin, central Taiwan: Quaternary International, v. 147, n. 1, p. 16–33, https:10.1016/j.quaint.2005.09.003

Lin, B., Liu, Z., Eglinton, T. I., Kandasamy, S., Blattmann, T. M., Haghipour, N., Huang, K. F., and You, C. F., 2020, Island-wide variation in provenance of riverine sedimentary organic carbon: A case study from Taiwan: Earth and Planetary Science Letters, v. 539, p. 116238, https:10.1016/j.epsl.2020.116238

Liu, F., Chang, X., Liao, Z., and Yang, C., 2019, *n*-Alkanes as indicators of climate and vegetation variations since the last glacial period recorded in a sediment core from the northeastern South China Sea (SCS): Journal of Asian Earth Sciences, v. 171, p. 134–143, https:10.1016/j.jseaes.2018.09.018

Liu, J. T., and Lin, H. l., 2004, Sediment dynamics in a submarine canyon: A case of river–sea interaction: Marine Geology, v. 207, n. 1–4, p. 55–81, https:10.1016/j.margeo.2004.03.015

Liu, J. T., Hung, J. J., Lin, H. L., Huh, C. A., Lee, C. L., Hsu, R. T., Huang, Y. W., and Chu, J. C., 2009, From suspended particles to strata: The fate of terrestrial substances in the Gaoping (Kaoping) submarine canyon: Journal of Marine Systems, v. 76, n. 4, p. 417–432, https:10.1016/j.jmarsys.2008.01.010

Liu, J. T., Liu, K. J., and Huang, J. C., 2002, The effect of a submarine canyon on the river sediment dispersal and inner shelf sediment movements in southern Taiwan: Marine Geology, v. 181, n. 4, p. 357–386, https:10.1016/S0025-3227(01)00219-5

Liu, J., Chen, J., Zhang, X., Li, Y., Rao, Z., and Chen, F., 2015, Holocene East Asian summer monsoon records in northern China and their inconsistency with Chinese stalagmite δ^{18}O records: Earth-Science Reviews, v. 148, p. 194–208, https:10.1016/j.earscirev.2015.06.004

Liu, W., and Huang, Y., 2005, Compound specific *D/H* ratios and molecular distributions of higher plant leaf waxes as novel paleoenvironmental indicators in the Chinese Loess Plateau: Organic Geochemistry, v. 36, n. 6, p. 851–860, https:10.1016/j.orggeochem.2005.01.006

Liu, Z., Colin, C., Li, X., Zhao, Y., Tuo, S., Chen, Z., Siringan, F. P., Liu, J. T., Huang, C.-Y., You, C. F., and Huang, K. F., 2010, Clay mineral distribution in surface sediments of the northeastern South China Sea and surrounding fluvial drainage basins: Source and transport: Marine Geology, v. 277, n. 1–4, p. 48–60, https:10.1016/j.margeo.2010.08.010

Liu, Z., Wen, X., Brady, E. C., Otto-Bliesner, B., Yu, G., Lu, H., Cheng, H., Wang, Y., Zheng, W., Ding, Y., Edwards, R. L., Cheng, J., Liu, W., and Yang, H., 2014, Chinese cave records and the East Asia Summer Monsoon: Quaternary Science Reviews, v. 83, p. 115–128, https:10.1016/j.quascirev.2013.10.021

Loughney, K. M., Hren, M. T., Smith, S. Y., and Pappas, J. L., 2020, Vegetation and habitat change in southern California through the Middle Miocene Climatic Optimum: Paleoenvironmental records from the Barstow Formation, Mojave Desert, USA: GSA Bulletin, v. 132, n. 1–2, p. 113–129, https:10.1130/B35061.1

Lourantou, A., Lavri⊠, J. V., Köhler, P., Barnola, J. M., Paillard, D., Michel, E., Raynaud, D., and Chappellaz, J., 2010, Constraint of the CO_2 rise by new atmospheric carbon isotopic measurements during the last deglaciation: Global Biogeochemical Cycles, v. 24, n. 2, https:10.1029/2009GB003545

Lüthi, D., Le Floch, M., Bereiter, B., Blunier, T., Barnola, J. M., Siegenthaler, U., Raynaud, D., Jouzel, J., Fischer, H., Kawamura, K., and Stocker, T. F., 2008, High-resolution carbon dioxide concentration record 650,000–800,000 years before present: Nature, v. 453, n. 7193, p. 379–382, https:10.1038/nature06949

Maher, B. A., and Thompson, R., 2012, Oxygen isotopes from Chinese caves: Records not of monsoon rainfall but of circulation regime: Journal of Quaternary Science, v. 27, n. 6, p. 615–624, https:10.1002/jqs.2553

McFarlin, J. M., Axford, Y., Masterson, A. L., and Osburn, M. R., 2019, Calibration of modern sedimentary δ^2H plant wax-water relationships in Greenland lakes: Quaternary Science Reviews, v. 225, p. 105978,https:10.1016/j.quascirev.2019.105978
Milliman, J. D., and Kao, S. J., 2005, Hyperpycnal discharge of fluvial sediment to the ocean: Impact of super-typhoon Herb (1996) on Taiwanese rivers: The Journal of Geology, v. 113, n. 5, p. 503–516, https:10.1086/431906
Milliman, J. D., and Syvitski, J. P. M., 1992, Geomorphic/Tectonic Control of Sediment Discharge to the Ocean: The Importance of Small Mountainous Rivers: The Journal of Geology, v. 100, n. 5, p. 525–544, https:10.1086/629606
Montgomery, D. R., and Dietrich, W. E., 1994, A physically based model for the topographic control on shallow landsliding: Water Resources Research, v. 30, n. 4, p. 1153–1171, https:10.1029/93WR02979
Nagamatsu, D., and Miura, O., 1997, Soil disturbance regime in relation to micro-scale landforms and its effects on vegetation structure in a hilly area in Japan: Plant Ecology, v. 133, n. 2, p. 191–200, https://doi.org/10.1023/A:1009743932202
Nusbaumer, J., Wong, T. E., Bardeen, C., and Noone, D., 2017, Evaluating hydrological processes in the Community Atmosphere Model Version 5 (CAM5) using stable isotope ratios of water: Journal of Advances in Modeling Earth Systems, v. 9, n. 2, p. 949–977, https:10.1002/2016MS000839
O'Leary, M. H., 1981, Carbon isotope fractionation in plants: Phytochemistry, v. 20, n. 4, p. 553–567, https:10.1016/0031-9422(81)85134-5
O'Leary, M. H., 1988, Carbon isotopes in photosynthesis: Fractionation techniques may reveal new aspects of carbon dynamics in plants: Bioscience, v. 38, n. 5, p. 328–336, https:10.2307/1310735
Oakes, A. M., and Hren, M. T., 2016, Temporal variations in the δD of leaf *n* -alkanes from four riparian plant species: Organic Geochemistry, v. 97, p. 122–130, https:10.1016/j.orggeochem.2016.03.010
Peltier, W. R., Argus, D. F., and Drummond, R., 2015, Space geodesy constrains ice age terminal deglaciation: The global ICE-6G_C (VM5a) model: Journal of Geophysical Research: Solid Earth, v. 120, n. 1, p. 450–487, https:10.1002/2014JB011176
Poage, M. A., and Chamberlain, C. P., 2001, Empirical relationships between elevation and the stable isotope composition of precipitation and surface waters: Considerations for studies of paleoelevation change: American Journal of Science, v. 301, n. 1, p. 1–15, https:10.2475/ajs.301.1.1
Polissar, P. J., Freeman, K. H., Rowley, D. B., McInerney, F. A., and Currie, B. S., 2009, Paleoaltimetry of the Tibetan Plateau from *D/H* ratios of lipid biomarkers: Earth and Planetary Science Letters, v. 287, n. 1–2, p. 64–76, https:10.1016/j.epsl.2009.07.037
Ponton, C., West, A. J., Feakins, S. J., and Galy, V., 2014, Leaf wax biomarkers in transit record river catchment composition: Geophysical Research Letters, v. 41, n. 18, p. 6420–6427, https://doi.org/10.1002/2014GL061328
Prentice, I. C., Meng, T., Wang, H., Harrison, S. P., Ni, J., and Wang, G., 2011, Evidence of a universal scaling relationship for leaf CO2 drawdown along an aridity gradient: New Phytologist, v. 190, n. 1, p. 169–180, https:10.1111/j.1469-8137.2010.03579.x
Risi, C., Bony, S., and Vimeux, F., 2008, Influence of convective processes on the isotopic composition (δ^{18}O and δD) of precipitation and water vapor in the tropics: 2. Physical interpretation of the amount effect: Journal of Geophysical Research-Atmospheres, v. 113, n. D19, https:10.1029/2008JD009943
Romans, B. W., Castelltort, S., Covault, J. A., Fildani, A., and Walsh, J. P., 2016, Environmental signal propagation in sedimentary systems across timescales: Earth-Science Reviews, v. 153, p. 7–29, https:10.1016/j.earscirev.2015.07.012
Rowley, D. B., Pierrehumbert, R. T., and Currie, B. S., 2001, A new approach to stable isotope-based paleoaltimetry: Implications for paleoaltimetry and paleohypsometry of the High Himalaya since the Late Miocene: Earth and Planetary Science Letters, v. 188, n. 1–2, p. 253–268, https:10.1016/S0012-821X(01)00324-7
Rozanski, K., and Araguás-Araguás, L., and Gonfiantini, R., 1993, Isotopic patterns in modern global precipitation: Climate Change in Continental Isotopic Records, v. 78, p. 1–36, https://doi.org/10.1029/GM078p0001
Sachse, D., Billault, I., Bowen, G. J., Chikaraishi, Y., Dawson, T. E., Feakins, S. J., Freeman, K. H., Magill, C. R., McInerney, F. A., van der Meer, M. T. J., Polissar, P., Robins, R. J., Sachs, J. P., Schmidt, H. L., Sessions, A. L., White, J. W. C., West, J. B., and Kahmen, A., 2012, Molecular Paleohydrology: Interpreting the Hydrogen-Isotopic Composition of Lipid Biomarkers from Photosynthesizing Organisms: Annual Review of Earth and Planetary Sciences, v. 40, n. 1, p. 221–249, https:10.1146/annurev-earth-042711-105535
Schubert, B. A., and Jahren, A. H., 2012, The effect of atmospheric CO_2 concentration on carbon isotope fractionation in C_3 land plants: Geochimica et Cosmochimica Acta, v. 96, p. 29–43, https:10.1016/j.gca.2012.08.003
Schubert, B. A., and Jahren, A. H., 2015, Global increase in plant carbon isotope fractionation following the Last Glacial Maximum caused by increase in atmospheric pCO_2: Geology, v. 43, n. 5, p. 435–438, https:10.1130/G36467.1
Seki, O., Nakatsuka, T., Shibata, H., and Kawamura, K., 2010, A compound-specific *n*-alkane δ^{13}C and δD approach for assessing source and delivery processes of terrestrial organic matter within a forested watershed in northern Japan: Geochimica et Cosmochimica Acta, v. 74, n. 2, p. 599–613, https:10.1016/j.gca.2009.10.025
Shyu, J. B. H., ms, 1999, The sedimentary environment of southern Pingdong plain since the last glacial (in Chinese with English abstract): Taiwan, National Taiwan University, M. S. thesis, 212 p.

Steiger, N. J., Steig, E. J., Dee, S. G., Roe, G. H., and Hakim, G. J., 2017, Climate reconstruction using data assimilation of water isotope ratios from ice cores: Journal of Geophysical Research: Atmospheres, v. 122, n. 3, p. 1545–1568, https:10.1002/2016JD026011

Steinke, S., Mohtadi, M., Groeneveld, J., Lin, L. C., Löwemark, L., Chen, M. T., and Rendle-Bühring, R., 2010, Reconstructing the southern South China Sea upper water column structure since the Last Glacial Maximum: Implications for the East Asian winter monsoon development: Paleoceanography and Paleoclimatology, v. 25, n. 2, p. PA2219,https:10.1029/2009PA001850

Steinke, S., Glatz, C., Mohtadi, M., Groeneveld, J., Li, Q., and Jian, Z., 2011, Past dynamics of the East Asian monsoon: No inverse behaviour between the summer and winter monsoon during the Holocene: Global and Planetary Change, v. 78, n. 3–4, p. 170–177, https:10.1016/j.gloplacha.2011.06.006

Tabor, C., Otto-Bliesner, B., and Liu, Z., 2020, Speleothems of South American and Asian Monsoons Influenced by a Green Sahara: Geophysical Research Letters, v. 47, n. 22, p.e2020GL089695, https:10.1029/2020GL089695

Tabor, C. R., and Otto-Bliesner, B. L., Brady, E. C., Nusbaumer, J., Zhu, J., Erb, M. P., Wong, T. E., Liu, Z., and Noone, D., 2018, Interpreting precession-driven $\delta^{18}O$ variability in the South Asian monsoon region: Journal of Geophysical Research: Atmospheres, v. 123, n. 11, p. 5927–5946, https:10.1029/2018JD028424

Teunissen van Manen, M. L., Jansen, B., Cuesta, F., León-Yánez, S., and Gosling, W. D., 2020, From leaf to soil: *n*-alkane signal preservation, despite degradation along an environmental gradient in the tropical Andes: Biogeosciences, v. 17, p. 5465–5487, https:10.5194/bg-17-5465-2020

Thomas, E. K., Clemens, S. C., Prell, W. L., Herbert, T. D., Huang, Y., Liu, Z., Sinninghe Damsté, J. S., Sun, Y., and Wen, X., 2014, Temperature and leaf wax δ^2H records demonstrate seasonal and regional controls on Asian monsoon proxies: Geology, v. 42, n. 12, p. 1075–1078, https:10.1130/G36289.1

Tierney, J. E., and DeMenocal, P. B., 2013, Abrupt Shifts in Horn of Africa Hydroclimate Since the Last Glacial Maximum: Science, v. 342, n. 6160, p. 843–846, https:10.1126/science.1240411

Tierney, J. E., Russell, J. M., Huang, Y., Damsté, J. S. S., Hopmans, E. C., and Cohen, A. S., 2008, Northern Hemisphere Controls on Tropical Southeast African Climate During the Past 60,000 Years: Science, v. 322, n. 5899, p. 252–255, https:10.1126/science.1160485

Tipple, B. J., Meyers, S. R., and Pagani, M., 2010, Carbon isotope ratio of Cenozoic CO_2: A comparative evaluation of available geochemical proxies: Paleoceanography and Paleoclimatology, v. 25, n. 3, p. 1–11, https:10.1029/2009PA001851

Vogts, A., Moossen, H., Rommerskirchen, F., and Rullkötter, J., 2009, Distribution patterns and stable carbon isotopic composition of alkanes and alkan-1-ols from plant waxes of African rain forest and savanna C_3 species: Organic Geochemistry, v. 40, n. 10, p. 1037–1054, https:10.1016/j.orggeochem.2009.07.011

Wang, C., Eley, Y., Oakes, A., and Hren, M., 2017, Hydrogen isotope and molecular alteration of *n*-alkanes during heating in open and closed systems: Organic Geochemistry, v. 112, p. 47–58, https:10.1016/j.orggeochem.2017.07.006

Wang, J., Howarth, J. D., McClymont, E. L., Densmore, A. L., Fitzsimons, S. J., Croissant, T., Gröcke, D. R., West, M. D., Harvey, E. L., Frith, N. V., Garnett, M. H., and Hilton, R. G., 2020, Long-term patterns of hillslope erosion by earthquake-induced landslides shape mountain landscapes: Science Advances, v. 6, n. 23, p. eaaz6446, https:10.1126/sciadv.aaz6446

Wang, Y. J., Cheng, H., Edwards, R. L., An, Z. S., Wu, J. Y., Shen, C.-C., and Dorale, J. A., 2001, A High-Resolution Absolute-Dated Late Pleistocene Monsoon Record from Hulu Cave, China: Science, v. 294, n. 5550, p. 2345–2348, https:10.1126/science.1064618

Wang, Y. V., Larsen, T., Leduc, G., Andersen, N., Blanz, T., and Schneider, R. R., 2013, What does leaf wax δD from a mixed C_3/C_4 vegetation region tell us?: Geochimica et Cosmochimica Acta, v. 111, p. 128–139, https:10.1016/j.gca.2012.10.016

Warren, C. R., McGrath, J. F., and Adams, M. A., 2001, Water availability and carbon isotope discrimination in conifers: Oecologia, v. 127, n. 4, p. 476–486, https:10.1007/s004420000609

Wong, T. E., Nusbaumer, J., and Noone, D. C., 2017, Evaluation of modeled land-atmosphere exchanges with a comprehensive water isotope fractionation scheme in version 4 of the Community Land Model: Journal of Advances in Modeling Earth Systems, v. 9, n. 2, p. 978–1001, https:10.1002/2016MS000842

Yang, T. N., Lee, T. Q., Meyers, P. A., Song, S. R., Kao, S. J., Löwemark, L., Chen, R. F., Chen, H. F., Wei, K. Y., Fan, C. W., Shiau, L. J., Chiang, H. W., Chen, Y. G., and Chen, M. T., 2011, Variations in monsoonal rainfall over the last 21 kyr inferred from sedimentary organic matter in Tung-Yuan Pond, southern Taiwan: Quaternary Science Reviews, v. 30, n. 23–24, p. 3413–3422, https:10.1016/j.quascirev.2011.08.017

Yu, S. W., Tsai, L. L., Talling, P. J., Lin, A. T., Mii, H. S., Chung, S. H., and Horng, C.-S., 2017, Sea level and climatic controls on turbidite occurrence for the past 26 kyr on the flank of the Gaoping Canyon off SW Taiwan: Marine Geology, v. 392, p. 140–150, https:10.1016/j.margeo.2017.08.011

Zhang, J., Liu, Z., Brady, E. C., Oppo, D. W., Clark, P. U., Jahn, A., Marcott, S. A., and Lindsay, K., 2017, Asynchronous warming and $\delta^{18}O$ evolution of deep Atlantic water masses during the last deglaciation: Proceedings of the National Academy of Sciences of the United States of America, v. 114, n. 42, p. 11075–11080, https:10.1073/pnas.1704512114

Zhang, Y., Liu, Z., Zhao, Y., Colin, C., Zhang, X., Wang, M., Zhao, S., and Kneller, B., 2018, Long-term *in situ* observations on typhoon-triggered turbidity currents in the deep sea: Geology, v. 46, n. 8, p. 675–678, https:10.1130/G45178.1

Zhou, B., Zheng, H., Yang, W., Taylor, D., Lu, Y., Wei, G., Li, L., and Wang, H., 2012, Climate and vegetation variations since the LGM recorded by biomarkers from a sediment core in the northern South China Sea: Journal of Quaternary Science, v. 27, n. 9, p. 948–955, https:10.1002/jqs.2588

Zhu, J., Liu, Z., Brady, E., and Otto-Bliesner, B., Zhang, J., Noone, D., Tomas, R., Nusbaumer, J., Wong, T., Jahn, A., and Tabor, C., 2017, Reduced ENSO variability at the LGM revealed by an isotope-enabled Earth system model: Geophysical Research Letters, v. 44, n. 13, p. 6984–6992, https:10.1002/2017GL073406

Zhuang, G., Brandon, M. T., Pagani, M., and Krishnan, S., 2014, Leaf wax stable isotopes from Northern Tibetan Plateau: Implications for uplift and climate since 15 Ma: Earth and Planetary Science Letters, v. 390, p. 186–198, https:10.1016/j.epsl.2014.01.003

Zhuang, G., Pagani, M., Chamberlin, C., Strong, D., and Vandergoes, M., 2015, Altitudinal shift in stable hydrogen isotopes and microbial tetraether distribution in soils from the Southern Alps, NZ: Implications for paleoclimatology and paleoaltimetry: Organic Geochemistry, v. 79, p. 56–64, https:10.1016/j.orggeochem.2014.12.007